



**HAL**  
open science

## **Cav3.2 T-type calcium channels shape electrical firing in mouse Lamina II neurons**

Miriam Candelas, Ana Reynders, Margarita Arango-Lievano, Christoph Neumayer, Antoine Fruquière, Elsa Demes, Jawed Hamid, Céline Lemmers, Claire Bernat, Arnaud Monteil, et al.

### **► To cite this version:**

Miriam Candelas, Ana Reynders, Margarita Arango-Lievano, Christoph Neumayer, Antoine Fruquière, et al.. Cav3.2 T-type calcium channels shape electrical firing in mouse Lamina II neurons. *Scientific Reports*, 2019, 9 (1), 10.1038/s41598-019-39703-3 . hal-02356250

**HAL Id: hal-02356250**

**<https://hal.science/hal-02356250v1>**

Submitted on 8 Nov 2019

**HAL** is a multi-disciplinary open access archive for the deposit and dissemination of scientific research documents, whether they are published or not. The documents may come from teaching and research institutions in France or abroad, or from public or private research centers.

L'archive ouverte pluridisciplinaire **HAL**, est destinée au dépôt et à la diffusion de documents scientifiques de niveau recherche, publiés ou non, émanant des établissements d'enseignement et de recherche français ou étrangers, des laboratoires publics ou privés.

# SCIENTIFIC REPORTS

OPEN

## Cav3.2 T-type calcium channels shape electrical firing in mouse Lamina II neurons

Miriam Candelas<sup>1,2,3,4</sup>, Ana Reynders<sup>5</sup>, Margarita Arango-Lievano<sup>2,3,4</sup>, Christoph Neumayer<sup>1,2,3,4</sup>, Antoine Fruquière<sup>1,2,3,4</sup>, Elsa Demes<sup>1,2,3,4</sup>, Jawed Hamid<sup>6</sup>, Céline Lemmers<sup>1,2,3,7</sup>, Claire Bernat<sup>1,2,3,7</sup>, Arnaud Monteil<sup>1,2,3,4,7</sup>, Vincent Compan<sup>1,2,3,4</sup>, Sophie Laffray<sup>1,2,3,4</sup>, Perrine Inquimbert<sup>8</sup>, Yves Le Feuvre<sup>9</sup>, Gerald W. Zamponi<sup>6</sup>, Aziz Moqrich<sup>5</sup>, Emmanuel Bourinet<sup>1,2,3,4</sup> & Pierre-François Méry<sup>1,2,3,4</sup>

The T-type calcium channel, Cav3.2, is necessary for acute pain perception, as well as mechanical and cold allodynia in mice. Being found throughout sensory pathways, from excitatory primary afferent neurons up to pain matrix structures, it is a promising target for analgesics. In our study, Cav3.2 was detected in ~60% of the lamina II (LII) neurons of the spinal cord, a site for integration of sensory processing. It was co-expressed with Tlx3 and Pax2, markers of excitatory and inhibitory interneurons, as well as nNOS, calretinin, calbindin, PKC $\gamma$  and not parvalbumin. Non-selective T-type channel blockers slowed the inhibitory but not the excitatory transmission in LII neurons. Furthermore, T-type channel blockers modified the intrinsic properties of LII neurons, abolishing low-threshold activated currents, rebound depolarizations, and blunting excitability. The recording of Cav3.2-positive LII neurons, after intraspinal injection of AAV-DJ-Cav3.2-mcherry, showed that their intrinsic properties resembled those of the global population. However, Cav3.2 ablation in the dorsal horn of Cav3.2<sup>GFP-Flox</sup> KI mice after intraspinal injection of AAV-DJ-Cav3.2-Cre-IRES-mcherry, had drastic effects. Indeed, it (1) blunted the likelihood of transient firing patterns; (2) blunted the likelihood and the amplitude of rebound depolarizations, (3) eliminated action potential pairing, and (4) remodeled the kinetics of the action potentials. In contrast, the properties of Cav3.2-positive neurons were only marginally modified in Cav3.1 knockout mice. Overall, in addition to their previously established roles in the superficial spinal cord and in primary afferent neurons, Cav3.2 channel appear to be necessary for specific, significant and multiple controls of LII neuron excitability.

Pain therapeutics act at various levels of the nociceptive pathway and of the pain matrix where they frequently target ion channels, or receptors. The constitutive deletion of the Cav3.2 gene, encoding a T-type calcium channel, alleviates acute pain, inflammatory pain, and visceral pain in mice<sup>1</sup>, suggesting its utility as a therapeutic target. Accordingly, T-type calcium channel antagonists induce various forms of analgesia in animals and humans<sup>2-4</sup>. Thus, it is important to define 1) loci of action of Cav3.2 antagonists *in vivo*, and 2) the mechanism of action of Cav3.2 on cellular functions within these loci along the nociceptive tract.

Pharmacological data support pre- and post-synaptic roles for T-type channels in the dorsal horn (DH) of the spinal cord where primary sensory inputs are first integrated and processed<sup>5-12</sup>. Because of limitations concerning the pharmacology of T-type channels, genetic approaches were required in determining the role of Cav3.2 channels in primary afferent neurons<sup>13-15</sup>. A pre-synaptic facilitation of glutamatergic transmission in superficial spinal cord neurons, that is absent in Cav3.2 knockout mice, is strengthened in a model of painful diabetic

<sup>1</sup>Laboratories of Excellence - Ion Channel Science and Therapeutics, Montpellier, France. <sup>2</sup>Inserm U-1191, Montpellier, France. <sup>3</sup>CNRS UMR 5203, Institut de Génomique Fonctionnelle, Montpellier, France. <sup>4</sup>Université Montpellier, Montpellier, France. <sup>5</sup>Aix-Marseille-Université, CNRS, Institut de Biologie du Développement de, Marseille, France. <sup>6</sup>Department of Physiology and Pharmacology, University of Calgary, Calgary, Canada. <sup>7</sup>Plateforme de Vectorologie, Biocampus Montpellier, CNRS UMS 3426, INSERM U5009, Montpellier, France. <sup>8</sup>CNRS, Institut des Neurosciences Cellulaires et Intégratives, Strasbourg, France. <sup>9</sup>UMR 5297, Interdisciplinary Institute for Neuroscience, Bordeaux, France. Correspondence and requests for materials should be addressed to E.B. (email: [emmanuel.bourinet@igf.cnrs.fr](mailto:emmanuel.bourinet@igf.cnrs.fr)) or P.-F.M. (email: [pierre-francois.mery@igf.cnrs.fr](mailto:pierre-francois.mery@igf.cnrs.fr))

neuropathy<sup>10</sup>. The intrathecal injection of Cav3.2 antisense shRNA blunts visceral pain<sup>16</sup>, has an anti-allodynic effect in a neuropathic pain model in rats<sup>17</sup> and an anti-hyperalgesic effect in diabetic rats<sup>18</sup>. When restricted to Nav1.8-expressing primary afferent neurons, the conditional ablation of Cav3.2 also has a variety of effects, including a diminution in noxious cold perception, a reduction in chemical nociception and an anti-allodynic effect in chronic pain models<sup>14</sup>. Of note, the anti-allodynic effect of Cav3.2 deletion in non-myelinated fibers involves C-LTMR afferent fibers that project to lamina II, LII<sup>14,19,20</sup>. Thus, there is evidence for a role of Cav3.2 in the pathophysiology of primary sensory neurons. Post-synaptic Cav3.2 channels should be investigated within spinal cord networks as well, since Cav3.2 expression is found in lamina II-IV interneurons<sup>13–15</sup>. This region is well-known to receive descending nociceptive controls to gate sensory flow within the spinal cord, and to undergo disinhibition during allodynia<sup>20–26</sup>. Yet, some unidentified LII interneurons can express T-type channels<sup>14,27</sup>, and can exhibit T-type dependent activity<sup>12,28–32</sup>.

Here we show that Cav3.2 channels are broadly expressed in a heterogeneous population of LII neurons. An examination of the electrophysiological properties of unidentified neurons revealed a strong sensitivity of rebound depolarization to TTA-A2, a T-type channel inhibitor. Using a viral based cell identification strategy, we next focused on Cav3.2-expressing neurons, which exhibited electrophysiological properties close to those of the whole population. A Cre-recombinase induced deletion of Cav3.2 in adult mice changed the distribution of firing patterns, the properties of the action potential and eliminated the pairing of action potentials in LII neurons exhibiting a rebound behavior. Collectively, our findings reveal important functions for Cav3.2 in the processing of sensory information within the spinal cord.

## Materials and Methods

**Study approval.** Animal procedures (#747) complied with the welfare guidelines of the European Community and were ethically approved by the Direction of Veterinary departments of Hérault, France (Agreement Number A 34-172-41).

**Slice preparation for electrophysiological recordings.** Adult 6–12 week-old wildtype or Cav3.2<sup>GFP-Flox</sup> KI mice<sup>14</sup> were anesthetized by injection of 0.1 ml/10 g ketamine (10 mg/ml) plus xylazine (1 mg/ml). They were perfused through the left ventricle with solution-1 [in mM; 122 N-Methyl-D-glucamine-Cl, 2.5 KCl, 1 CaCl<sub>2</sub>, 7 MgCl<sub>2</sub>, 2.5 NaHCO<sub>3</sub>, 1.5 NaH<sub>2</sub>PO<sub>4</sub>, 10 HEPES, 25 glucose, 0.2–5 ascorbic acid, 0.2–5 thiourea; pH 7.4, 0–2 °C, gassed with O<sub>2</sub>]<sup>33</sup>. N-Acetyl-L-cysteine 2 mM was added when studying mice aged 10–12 weeks. The lumbar region of the spinal cord was quickly removed in solution-1, embedded into low-melting agarose and 300 μm-thick frontal sections were processed on a microtome (Leica VT12000S, Leica Microsystem, Nanterre, France) within 20 min and kept at least for 1 hour in solution-2 [in mM; 115 NaCl, 2.5 KCl, 2 CaCl<sub>2</sub>, 4 MgCl<sub>2</sub>, 26 NaHCO<sub>3</sub>, 1.25 NaH<sub>2</sub>PO<sub>4</sub>, 25 glucose, 0.2 ascorbic acid, 0.2 thiourea; pH 7.4, 30 °C, gassed with 95% CO<sub>2</sub>-5% O<sub>2</sub>].

**Patch-clamp recordings.** Slices were immobilized with a nylon grid in a submersion chamber on the stage of an upright microscope (Olympus BX51WIF, Olympus Fr., Rungis, France) and superfused with solution-3 [in mM; 125 NaCl, 2.5 KCl, 2 CaCl<sub>2</sub>, 1 MgCl<sub>2</sub>, 26 NaHCO<sub>3</sub>, 1.25 NaH<sub>2</sub>PO<sub>4</sub>, 11 glucose; pH 7.4, 32 °C, gassed with 95% CO<sub>2</sub>-5% O<sub>2</sub>] at 2 ml/min for at least 15 min. Infrared differential interference contrast illumination was used to visualize neurons, with a x40 immersion objective and Nomarski differential interference contrast optics, and the images captured with a camera (Jenoptik ProgRes MF, Bayeux, France). When appropriate, the mCherry fluorescent signal was superimposed with the IR-DIC image in order to locate the Cav3.2-expressing neurons. Borosilicate glass pipettes were connected to the head stage of a Axon MultiClamp 700B, interfaced with an Axon Digidata 1550A and controlled with pClamp10 (all from Molecular Devices, Sunnyvale, USA). Drugs were either bath-applied or puff-applied locally. When bath-applied, solutions were changed by switching the supply of the superfusion system. When puff-applied in the vicinity of the neurons with a pipette, compounds were diluted in a HEPES-based medium containing in mM: 138 NaCl, 2.5 KCl, 2 CaCl<sub>2</sub>, 1 MgCl<sub>2</sub>, 3 NaHCO<sub>3</sub>, 1.25 NaH<sub>2</sub>PO<sub>4</sub>, 10 HEPES, 12 glucose, pH 7.4 with NaOH. Atto-dye 550 or Atto-dye 488 (Invitrogen, Waltham, USA) were occasionally included in the ejection pipette as a control. Slices were discarded after being exposed to a compound. All chemicals were obtained from Sigma-Aldrich (L'isle d'Abeau, France) excepted TTA-A2 kindly provided by Merck Research Labs (West Point, PA, USA).

For action potential recordings and for glutamatergic currents recordings, pipettes (6–8 MΩ) were filled with (in mM): 139 K-gluconate, 10 HEPES, 0.1 EGTA acid, 1 MgCl<sub>2</sub>, 2 MgATP, 0.5 Na-GTP, 5 Na<sub>2</sub>-phosphocreatine, 2.5 Na-pyruvate, 2 malate, pH 7.3 with KOH (295 mOsm adjusted with KMeSO<sub>3</sub>). Atto-dye (550 or 488) was included in order to verify the identity of the neuron. Action potentials and resting properties were elicited by increasing and decreasing 2s-duration current pulses, respectively, from a holding adjusted at −70 mV<sup>34</sup>. Subthreshold electrical activity was triggered from −90 mV for 3 s to step-by-step current increments of 1.5 s until electrical activity was elicited<sup>32</sup>. Miniature glutamatergic currents were recorded in the presence of extracellular tetrodotoxin (TTX) 500 nM (Latoxan) at a holding potential of −70 mV. Analysis were performed with Axograph<sup>35</sup> or Clampex10 (Molecular Devices) using either a threshold based detection or an appropriate template.

This procedure was adapted for the recordings of T-type currents and for GABAergic current recordings. The internal solution was (in mM)<sup>36</sup>: 125 CsMeSO<sub>3</sub>, 10 HEPES, 5 EGTA acid, 1 MgCl<sub>2</sub>, 2 MgATP, 0.5 Na-GTP, 5 Na<sub>2</sub>-phosphocreatine, 2 Na-pyruvate, 2 malate, 7 KCl, pH 7.4 with CsOH (295 mOsm adjusted with CsMeSO<sub>3</sub>). When recording T-type currents, the external medium also contained TTX (500 nM), 4-aminopyridine (4-AP, 1 mM), tetra-ethyl-ammonium (TEA, 10 mM) and ivabradine (1 μM). For current-voltage relationships, neurons were voltage-clamped at −90 mV and 1s-duration pulses of increasing amplitude were delivered by steps of 5 mV. For the voltage ramp protocol, after a 500 ms step at −100 mV, the voltage was increased linearly to 40 mV during 200 ms. When recording miniature GABAergic currents, the external solution was supplemented further with APV (50 μM), DNQX (30 μM) and neurons were voltage-clamped at 20 mV.

**Plasmid cloning and virus production.** The minimal Cav3.2 promoter used was based upon nucleotide sequence derived from mouse CACNA1H gene locus sequence (ENSMUSG00000024112). We purchased a mouse Cav3.2 promoter clone (MPRM 12993) from promoter clone library (GeneCopoeia) with additional restriction endonuclease sites Mlu I and BamHI at the 5' prime and 3' prime ends, respectively. This clone consists of 1462 nucleotides of the mouse Cav3.2 gene, with 1450 nucleotides 5' to Exon 1 and 12 nucleotides of the non-coding exon 1 of mouse Cav3.2 gene (ENSMUSG00000024112, see Supplementary Fig. S1). This sequence was subjected to online analysis for core promoter sequences (<http://gpminer.mbc.nctu.edu.tw/index.php>) to confirm the presence of TATA and CCAAT boxes as identified in the rat sequence<sup>37</sup>. This promoter fragment was isolated via restriction with MluI and BamHI from the original promoter clone (MPRM 12993) and sub cloned into pAAV-hSyn-hChR2(H134R)-mCherry (Addgene26976) using the same restriction sites (MluI and BamHI) to replace the hSyn promoter sequences with mouse Cav3.2 promoter sequence. The plasmid pAAV-Cav3.2-mCherry was cloned using pAAV-Cav3.2-hChR2-mCherry. A 1300 bp fragment was amplified by PCR with the forward primer ATTCTAGAAAGACGAAGCCGAGGC and the reverse primer AAGAATACCAGTCAATCTTTCACAA. The PCR product was cloned into pAAV-Cav3.2-hChR2-mCherry using the XbaI and AfeI restriction sites. The pAAV-Cav3.2-Cre-mCherry was obtained by cloning the mCherry-IRES-Cre sequence of the plasmid pAAV-EF1a-mCherry-IRES-Cre (Addgene 55632) into the vector pAAV-Cav3.2-mCherry using BamHI and EcoRI restriction sites.

The Viral production in HEK-293 cells was performed with the DJ-packaging system (Cell Biolabs) and purified on a heparin column according to (Morgenstern, Marongiu *et al.*<sup>38</sup>). Virus titers ( $>10^{11}$  copies/ml in the present study) were estimated by q-PCR using either the forward primer TTGTTCTCCACCTCCTTC and the reverse primer GCAACATAGCAACCTCAG ACC, or the forward primer ACTGTGTTTGCTGACGCAAC and the reverse primer AGCGAAAGTCCCGAAAG.

**Intraspinal injection of virus.** Mice were anesthetized with ketamine plus xylazine and placed on a heating sheet (37°C). A 2cm-long incision was performed at the level of the L1 vertebra. The spinal cord was exposed by removing the dorsal portion of the vertebra L1 using a laminectomy forceps<sup>39</sup> or by carefully bending the spine without further surgery<sup>40</sup>. A micro syringe held on a stereotaxic frame and filled with the virus suspension was positioned at the rostral-most portion of the exposed spinal cord, 500  $\mu$ m laterally with respect to the posterior median sulcus. Injections (800 nl) were performed at a depth of 150–300  $\mu$ m, at a rate of 100–200 nl/min. After careful retraction of the syringe, this operation was repeated at the caudal-most portion of the exposed spinal cord. The fascia and the skin were sutured before the mouse was transferred into a recovery cage for >4 hours, and postsurgical treatments were provided according to guidelines. This procedure did not increase inflammatory markers, 3–4 weeks after injection, as assessed by changes in the morphologies of astrocytes and microglial cells<sup>39,40</sup>.

**Immunofluorescence experiments.** Mice (8–14 weeks) were anesthetized with ketamine plus xylazine and processed as follows<sup>14</sup>. Spinal cord were fixed with a transcardiac perfusion of cold PBS containing PFA 4% and a post-fixation (<2 hours) at 4°C. They were embedded in 4% agarose and sectioned at 30–40  $\mu$ m with a vibratome (Microm HM 650 V, Brignais, France). The sections were blocked with TBS plus 0.05% tween 20 (TBST), 0.2% Triton X 100 and 10% normal serum (goat or donkey), 22°C, for 1 hr; the incubations with primary antibodies (Supplementary Table 1) were done in blocking solution at 4°C overnight; and the incubation with secondary antibodies (Supplementary Table 1) were performed at 22°C, 2 hrs. They were included in Dako Mounting Medium (Agilent Tech., Santa Clara, USA) and images were performed on a confocal microscope (Leica SP8-UV, Nanterre, France) with x40 (Plan Apochromat 1.3 NA oil DIC) and x63 (Plan Apochromat 1.4 NA oil DIC) objectives. Image processing was performed with Fiji<sup>41</sup>, and cell densities were normalized to DAPI labelling or to the appropriate antigen as stated in the text.

**In situ hybridization and immunostaining.** *In situ* hybridization (ISH) and immunostaining were performed according to Moqrich *et al.*<sup>42</sup>. For ISH, all the probes were designed as follows: (i) Transcript-specific regions were determined using Blastn (NCBI) software and specific primers (Supplementary Table 2) were designed accordingly using PrimerBlast (NCBI) software. (ii) One first PCR was performed using the GoTaq Hot-Start polymerase kit (Promega) and cDNA templates from adult mouse dorsal root ganglia (for Cav 3.2 and 3.3) or hippocampus (for Cav3.1). (iii) A second PCR was performed, in which the product of the first PCR was used as template and the T7 RNA polymerase promoter sequence was fused to the reverse primer. (iv) RNA antisense probes were synthesized using the T7 RNA polymerase (Promega) and digoxigenin (DIG)-labelling system from Roche. Mice were deeply anesthetized with a mix of ketamine/xylazine and then transcardially perfused with an ice-cold solution of 4% PFA in PBS. After dissection, spinal cords were post-fixed for 12 h at 4°C and transferred into a 30% (w/v) sucrose solution for cryoprotection before being embedded in Optimal Cutting Temperature compound (Leica), then snap-frozen on dry ice and stored at –80°C. Sixteen to 18  $\mu$ m cryosections were obtained using a standard cryostat (Leica). Probes were hybridized overnight at 55°C, and the slides incubated with the horseradish peroxidase anti-digoxigenin antibody (Roche). Final detection was achieved using Cy3 TSA plus kit (Perkin Elmer). Sections were then incubated overnight at 4°C with the appropriate antibody (anti-RFP for mCherry, or rabbit anti-PKC $\gamma$ ), diluted in PBS supplemented with 10% (v/v) donkey serum (Sigma), 3% (w/v) bovine albumin (Sigma) and 0.4% (v/v) Triton X-100. Anti-rabbit Alexa Fluor 488 or anti-rabbit Alexa Fluor 647 antibodies (Supplementary Table 1) were used for secondary detection. Nuclei were stained with Hoechst (Sigma Aldrich). Slides were mounted with Immu-Mount (Thermo Scientific) prior to observation under LSM780 confocal microscope (Carl Zeiss, Jena, Germany). Contrast was adjusted using Photoshop software.



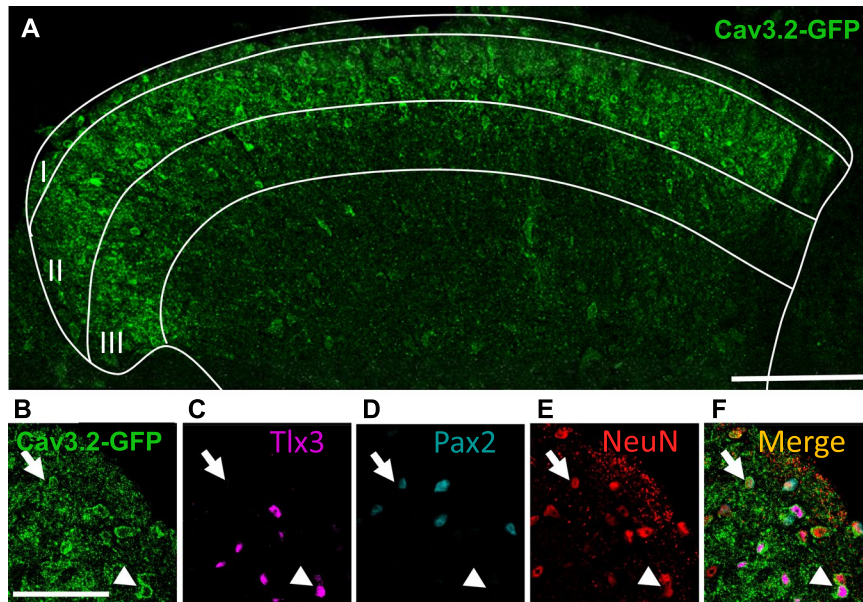


**Figure 1.** GFP immunofluorescence in the spinal cord of the adult Cav3.2<sup>GFP-Flox</sup> KI mouse. (A) Immunostaining for GFP (green), showing the localization of Cav3.2-GFP expressing cell bodies and neuronal fibers in the dorsal horn of the lumbar spinal cord. The majority of GFP is found in the upper layers of the dorsal horn. Coexpression of GFP ((B) green) with either Tlx3 ((C) purple, arrow), or Pax2 ((D) blue, arrowhead) and NeuN ((E) red), as well as the superimposition of the four images (F). Scale bars: (A) (100  $\mu$ m), (B–F) (25  $\mu$ m).

% of GFP-expressing neurons			% of neurons	
NeuN (8)	Tlx3 (15)	Pax2 (4)	Tlx3 (14)	Pax2 (3)
85.3 $\pm$ 5.2	70.8 $\pm$ 2.6	13.1 $\pm$ 4.7	47.5 $\pm$ 2.69	12.6 $\pm$ 6.1

**Table 1.** Coexpression of GFP with neuronal markers in Cav3.2<sup>GFP-Flox</sup> KI mice. Numbers are the mean  $\pm$  SEM of GFP-expressing neurons. Number of mice are indicated within brackets.

**Statistics.** Data were generally expressed as mean  $\pm$  SEM. In few cases, families of individual values are shown. They were compared with the appropriate tests using Prism, and  $p < 0.05$  was considered as significantly different. The numbers of neurons and mice studied using the patch-clamp techniques are summarized in Supplementary Tables 3 and 4.

## Results

**Distribution of cells expressing Cav3.2-GFP and neurochemical phenotype.** To determine the nature of Cav3.2-expressing cell types in the spinal cord, we took advantage of Cav3.2<sup>GFP-Flox</sup> KI mice that express GFP at the Cav3.2 locus<sup>13</sup>. In adult Cav3.2<sup>GFP-Flox</sup> KI mice, GFP labelled cell bodies and nerve terminals mostly located in LII of the spinal cord (Fig. 1A), as previously reported<sup>14</sup>. The majority of GFP-positive cell bodies (about 70%) co-expressed Tlx3, a marker of excitatory neurons (Fig. 1B,C). A small fraction (about 13%) of GFP-positive cell bodies were positive for Pax2, a marker of inhibitory interneurons (Fig. 1B,D)<sup>43,44</sup>. The neuronal origin of GFP-expressing cells in the spinal cord was further confirmed using pan-neuronal NeuN staining (Fig. 1B,E and Table 1). Overall, Cav3.2 was present in about 60% of the LII neurons, contributing to about half of the Tlx3-positive subset (47.5%, Table 1) and to a much smaller subpopulation of Pax2-positive neurons (12.6%, Table 1).

Further dissection of neuronal cell types expressing Cav3.2 using immunolabelling for GFP and known markers of subpopulations of LII-LIII neurons involved in sensory processing by the DH (calbindin, CB; protein kinase C gamma, PKC $\gamma$ ; calretinin, CR; neuronal NOS, nNOS; parvalbumin, PV), revealed a heterogeneous expression pattern (Fig. 2, Table 2). Most of GFP-expressing neurons were CB-positive (43.2% of GFP neurons, Table 2, Fig. 2A) or PKC $\gamma$ -positive (37.0% of GFP neurons, Table 2, Fig. 2B), two markers of excitatory LII neurons<sup>19,20,45,46</sup>. The GFP-positive neurons expressing CB also expressed Tlx3 (40.3% of GFP neurons, Table 2), a marker of excitatory DH interneurons<sup>43</sup>. The GFP-positive neurons expressing PKC $\gamma$  were mainly excitatory since 85.7% of the PKC $\gamma$ -positive neurons expressed GFP, PKC $\gamma$  and Tlx3 (Table 2). Interestingly, most PKC $\gamma$ -expressing neurons, which are disinhibited during mechanical allodynia<sup>23,24,26</sup>, expressed Cav3.2 (91.7%, Fig. 2B, Table 2). Besides expressing Cav3.2, some PKC $\gamma$  interneurons could also express Cav3.1 and Cav3.3 mRNAs, as detected by *in situ* hybridization (Supplementary Fig. S2). Almost half of the CR neurons, which relay nociceptive inputs to projection neurons<sup>23,24</sup>, were GFP-positive (Fig. 2C, Table 2). This population was mostly excitatory, since CR labeling alone, and CR/Tlx3 double labelling represented 26.1% and 22.1%, of the GFP-positive neurons, respectively

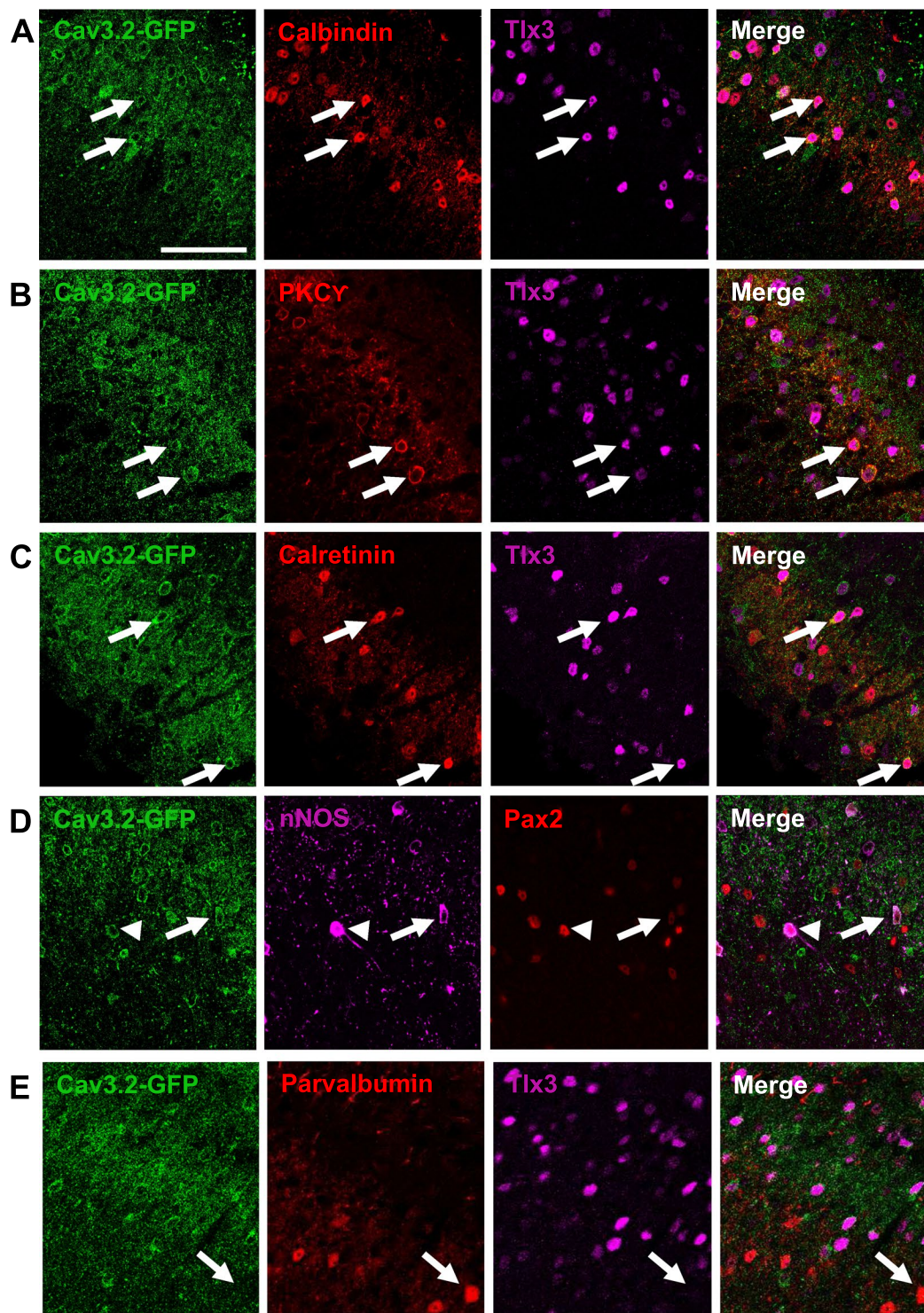


**Figure 2.** GFP labeled a heterogeneous population in the LII of Cav3.2<sup>GFP-Flox</sup> KI mice. GFP (green) was coexpressed with calbindin (A), PKC $\gamma$  (B), calretinin (C), nNOS (D), but not with parvalbumin (E). These neurons were either excitatory, Tlx3-positive (arrows, (A–C,E)) and Pax2-negative (arrow, (D)); or inhibitory, Pax2-positive (arrowhead, (C)). Scale bar: 50  $\mu$ m.

(Table 2). A small subset of GFP-expressing neurons also expressed nNOS (10.7%), and they accounted for almost half of the nNOS-positive neurons (42.1%, Fig. 2D, Table 2). These neurons, are both inhibitory and excitatory (Table 2), in agreement with a previous report<sup>47</sup> and are differentially recruited during noxious stimulations<sup>48</sup>. In contrast, the PV-expressing neurons of LIII, some of which are gatekeepers of the gate control theory for mechanical allodynia<sup>26</sup> were marginally GFP-positive (7.4% of the PV neurons, Fig. 2E, Table 2). Altogether, these results



CB	CB/Tlx3	PKC $\gamma$	PKC $\gamma$ / Tlx3	CR	CR/Tlx3	nNOS	nNOS/ Pax2	PV
<b>% of GFP-positive neurons</b>								
45 ± 5.5 (n = 5)	40.2 ± 5.1 (n = 5)	39.7 ± 5.6 (n = 6)	43.0 ± 4.2 (n = 4)	22.5 ± 5.7 (n = 5)	22 ± 4 (n = 4)	10.7 ± 2.8 (n = 4)	1.8 ± 1.8 (n = 2)	1.6 ± 1.1 (n = 3)
<b>% of neurons</b>								
46.25 ± 5 (n = 5)	69.37 ± 7.4 (n = 5)	89.5 ± 2.2 (n = 6)	85.7 ± 1.3 (n = 4)	41.1 ± 8.5 (n = 5)	36.1 ± 6.4 (n = 4)	42.1 ± 14.4 (n = 4)	20.3 ± 20 (n = 2)	7.6 ± 1.1 (n = 3)

**Table 2.** Coexpression of GFP with markers of the LII in adult Cav3.2<sup>GFP-Flox</sup> KI mice. Numbers are the mean ± SEM of GFP-expressing neurons. Number of mice are indicated within brackets. Counts for nNOS, calretinin (CR) and calbindin (CB) were limited to LII, while they also included the outer part of LIII in the case of PKC $\gamma$  and parvalbumin (PV).

indicate that Cav3.2 channels are expressed in a wide variety of spinal cord neurons, which relay primary afferent activity to projection neurons during mechanical allodynia.

**Effects of T-type channel inhibition on synaptic transmission.** The Cav3.2-expressing primary afferent neurons project to internal LII where most Cav3.2 neurons are found<sup>14</sup>. To study the T-type channel contribution to neurotransmission, we examined the synaptic currents in acute spinal cord slices from adult mice using whole cell patch clamp. Miniature excitatory post-synaptic currents (mEPSCs) of LII neurons were recorded at a membrane potential of  $-70$  mV<sup>49</sup>, in the presence of a sodium channel blocker (TTX 500 nM, Fig. 3). Addition of the T-type blocker TTA-A2 (500 nM) in the superfusion medium did not modify the mEPSCs in the experiment of Fig. 3A,B. On average, TTA-A2 had no effect of the mean distributions of either the amplitudes or the inter-event intervals of mEPSCs ( $n = 12$ , Fig. 3C,D). Another T-type channel blocker, NiCl<sub>2</sub> (100  $\mu$ M) also did not change the mean glutamatergic neurotransmission (Supplementary Fig. S3A,B). In addition, TTA-A2 did not significantly modify the spontaneous mEPSCs over time in the continuing presence of the HCN inhibitor ivabradine (1  $\mu$ M,  $n = 9$ , Supplementary Fig. S3C,D) or under constant GABA<sub>A</sub>-ergic (Gabazine 3  $\mu$ M) and Glycinergic (strychnine 3  $\mu$ M) receptor inhibition ( $n = 5$ , Supplementary Fig. S3E,F). In contrast, T-type channel blockade homogeneously inhibited the spontaneous GABAergic currents of LII neurons (Fig. 3E–H), as shown in a typical experiment where the puff application of TTA-A2 (1  $\mu$ M) altered the frequency of the miniature GABAergic currents recorded at 20 mV (Fig. 3E). On average, inter-event intervals (Fig. 3G), but not amplitudes (Fig. 3H), of GABAergic miniature currents were significantly diminished in the continuing presence of TTA-A2. Therefore, T-type channels participated in spontaneous inhibitory synaptic transmission, but not in the excitatory transmission of LII neurons. This does not exclude the possibility that T-type channels might exert significant contributions in some subpopulations of LII neurons<sup>11</sup>.

**Association of T-type channel activity with firing patterns of LII neurons.** T-type calcium channels participate in the intrinsic properties of some types of DH neurons<sup>12,29,30,32</sup>. Accordingly, voltage ramps or current-voltage relationships demonstrated the presence of low-voltage and high-voltage activated calcium currents in LII neurons, which could be, respectively, inhibited by NiCl<sub>2</sub> and CdCl<sub>2</sub> (Supplementary Fig. S4). Therefore, we analyzed the firing properties of LII neurons elicited by current pulses from a holding potential of  $-70$  mV in acute lumbar slices from adult mice (Supplementary Figs S5 and S6). The observed firing patterns were highly heterogeneous, with delayed firing profiles being the most frequent (28.5%), and various proportions of transient (18%), irregular tonic (16.5%), regular tonic (12.8%), gap firing (12.7%) and single spiking (11%) ( $n = 134$ , Supplementary Fig. S5C).

Subthreshold depolarizations elicited from a hyperpolarizing conditioning prepulse at  $-90$  mV were more homogeneous since three behaviors were observed: rebound (49%), hyperpolarizing (18%) and apparently passive decays (33%) ( $n = 124$ , Fig. 4A,B). Although these properties did not tightly segregate with a firing pattern ( $n = 124$ , Fig. 4C), neurons exhibiting rebounds more likely supported higher activities at the onset of the pulse, namely single spiking, transient and irregular tonic patterns. Since rebound shaped depolarizations can be a signature of T-type channel activity<sup>50</sup>, a multiple step protocol including a subthreshold and a suprathreshold current injection was designed to investigate the role of T-type channels on neuronal firing (Fig. 4D). When a neuron elicited a rebound depolarization, puff application of the T-type channel inhibitor TTA-A2 (1  $\mu$ M) significantly decreased the rebound amplitude during the first subthreshold step and abolished action potential firing during the second suprathreshold step ( $n = 7$ , Wilcoxon paired test,  $p = 0.01$ , Fig. 4E,F). Rebound depolarization was not only associated with an “all-or-none” effect on firing. Indeed, an analysis of the first five action potentials revealed that neurons exhibiting rebound depolarizations also specifically exhibited a pairing of the first two action potentials, (Fig. 4G,H), the inter-event interval of the second action potential being shorter than all others ( $n = 49$ , Wilcoxon paired tests, Fig. 4H). In neurons with a hyperpolarizing decay ( $n = 39$ ) and neurons with a passive response ( $n = 13$ ), the first action potential had the longest latency (Wilcoxon paired tests, Fig. 4H), and the next action potentials occurred regularly. Altogether, these data not only confirm the involvement of T-type calcium channels in the spinal cord, but show that they are mandatory for specific firing patterns.

**Properties of Cav3.2-expressing neurons in LII of the spinal cord.** Since the excitability of LII neurons appeared to be dependent on T-type calcium channels, a selective role for Cav3.2 was then investigated in greater detail. A 1.4 kb fragment of the Cav3.2 promoter gene was inserted into a pAAV expression vector in order to control the selective expression of the fluorescent protein mCherry in Cav3.2-expressing neurons. The viral

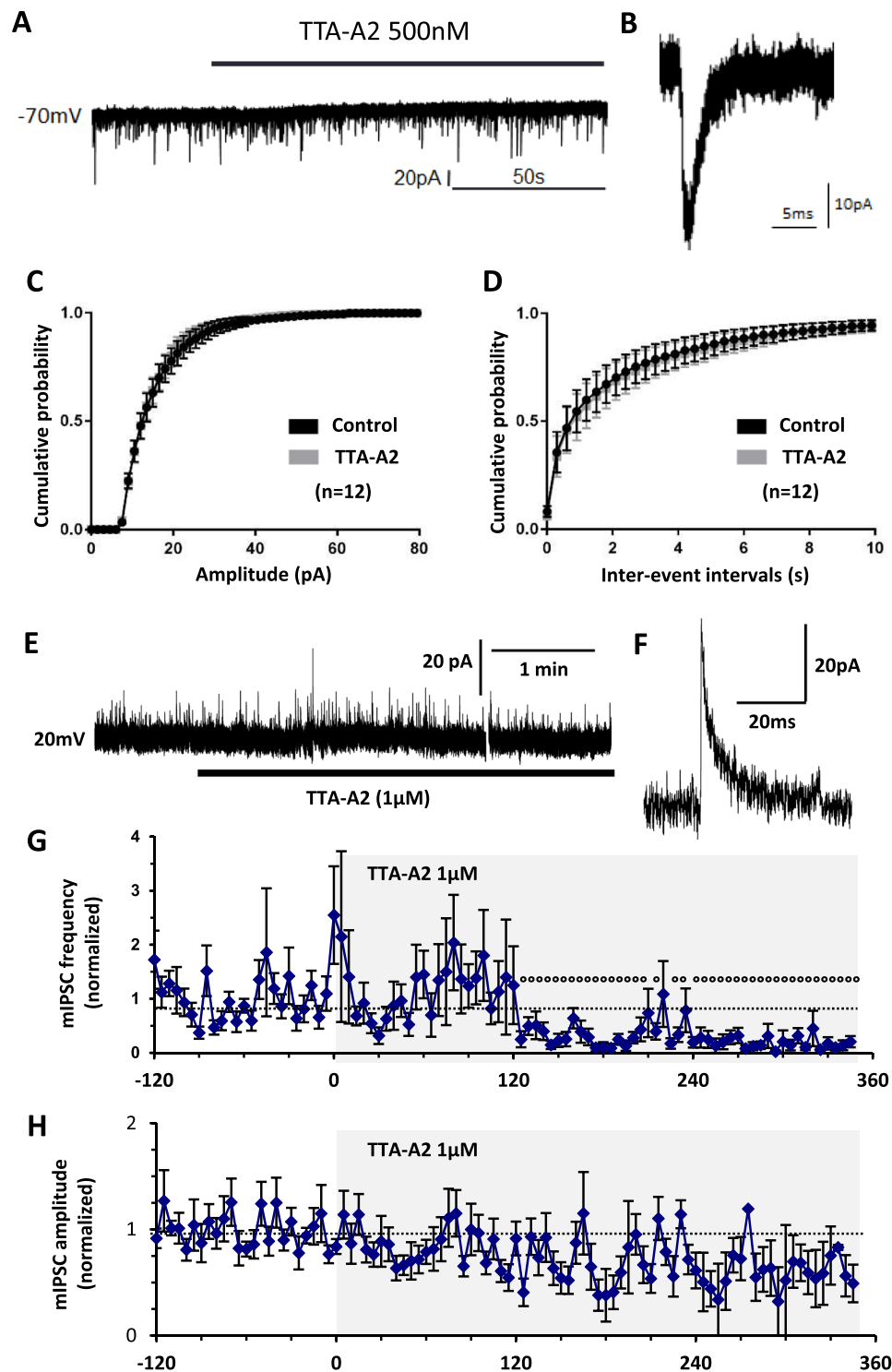


**Figure 3.** Effects of T-type calcium channel inhibitors on neurotransmission of LII neurons in the spinal cord of adult mice. (A) Typical whole cell patch clamp recording, performed in LII of an acute 300 $\mu$ m-thick slice taken from a lumbar segment of an adult mouse, showing miniature excitatory postsynaptic currents (mEPSC) of a neuron held at  $-70$  mV. (B) Trace showing an individual mEPSC. (C,D) Mean cumulative distribution of the amplitudes (C) and the inter-event intervals (D) of mEPSC in the absence (control) or presence of 500 nM TTA-A2 ( $n=12$ ). (E) Typical whole cell patch clamp recording, performed in LII of an acute 300 $\mu$ m-thick slice taken from a lumbar segment of an adult mouse, showing miniature inhibitory postsynaptic currents (mIPSC) of a neuron held at 20 mV. (F) Trace showing an individual mIPSC. (G,H) Mean frequencies (G) and amplitudes (H) of mIPSC in the absence and presence of 1  $\mu$ M TTA-A2 ejected at time 0, as shown by the grey area ( $n=12$ ).  $p < 0.05$ , paired student's t-test, is indicated as dots above symbols. Data were normalized to the mean of all the values recorded before time 0 (solid lines). At time 0, the raw frequency was  $0.59 \pm 0.17$  Hz, and the raw amplitude was  $17.4 \pm 1.6$  pA.



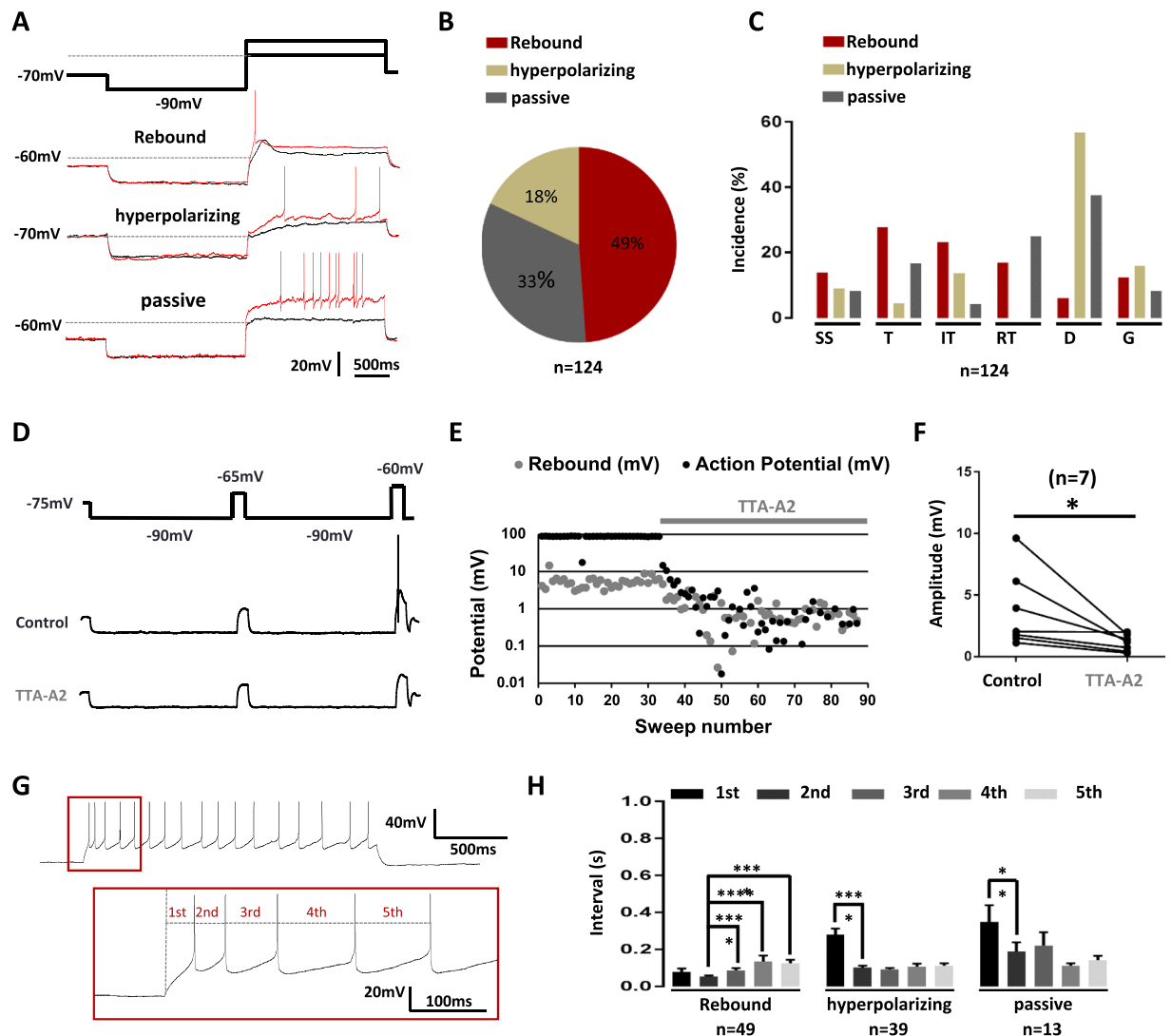


**Figure 4.** The rebound induced by hyperpolarization is T-type channel dependent. (A) A 2-step current clamp protocol with a hyperpolarizing prepulse to  $-90$  mV induced three kind of responses upon step by step depolarizations: rebound shaped, hyperpolarizing kinetics and passive depolarizations. Red traces show the firing at the rheobase. (B) Proportion of LII neurons exhibiting these three subthreshold activities. (C) Relationships between firing patterns and subthreshold behaviors. SS (Single spiking), T (Transient), IT (Irregular Tonic), RT (Regular Tonic), D (Delayed) and G (Gap). (D) Multi-steps protocol used in eliciting subthreshold (first depolarizing step) and supra-threshold activities (second depolarizing step), and typical recordings in the absence (control) and presence of TTA-A2. (E) Quantification of the effects of TTA-A2 puff application on the amplitude of the subthreshold and supra-threshold activities in a typical experiment in a LII neuron. (F) In all similar experiments, TTA-A2 ( $1 \mu\text{M}$ ) diminished the subthreshold rebound depolarization. (G) The intervals of the 5 first action potentials were quantified in LII neurons. (H) Mean intervals showed a pairing of the first two action potentials in neurons exhibiting rebound subthreshold activity. Bars are the means and lines are the SEM \*\*\*\* $p < 0.0001$ ; \*\*\* $p < 0.001$ ; \*\* $p < 0.01$ ; \* $p < 0.05$  using a Wilcoxon paired test.

particles were injected at two sites of the lumbar spinal cord in 4 weeks-old wildtype mice (Fig. 5A). Detection of mCherry-positive neurons by immunofluorescence 3–4 weeks after injection showed a large coverage of the lumbar segments in the rostrocaudal direction (Fig. 5B) that was specific for the ipsilateral side (Fig. 5C). The mCherry-positive neurons were also GFP-positive, after injection of the AAV-DJ-Cav3.2-mCherry virus in a Cav3.2<sup>GFP-Flox</sup> KI mouse (Fig. 5D). Similarly, the mCherry-positive neurons detected by immunofluorescence expressed Cav3.2 mRNA, as detected by *in situ* hybridization, after injection of the AAV-DJ-Cav3.2-mCherry virus in a wildtype mouse (Fig. 5E). On average, the Cav3.2-promoter driven expression of mCherry was found in 82% of the Cav3.2-GFP positive neurons, and in 93% of the Cav3.2 mRNA-expressing neurons (Fig. 5F). Thus, it faithfully reported Cav3.2 expression with a bright fluorescence signal.

Having established and validated a novel tool for identifying Cav3.2-expressing neurons, we were able to investigate their firing properties in wildtype mice that had been injected with the AAV-DJ-Cav3.2-mCherry virus. Voltage clamp experiments elicited typical T-type calcium currents from a holding potential of  $-90$  mV

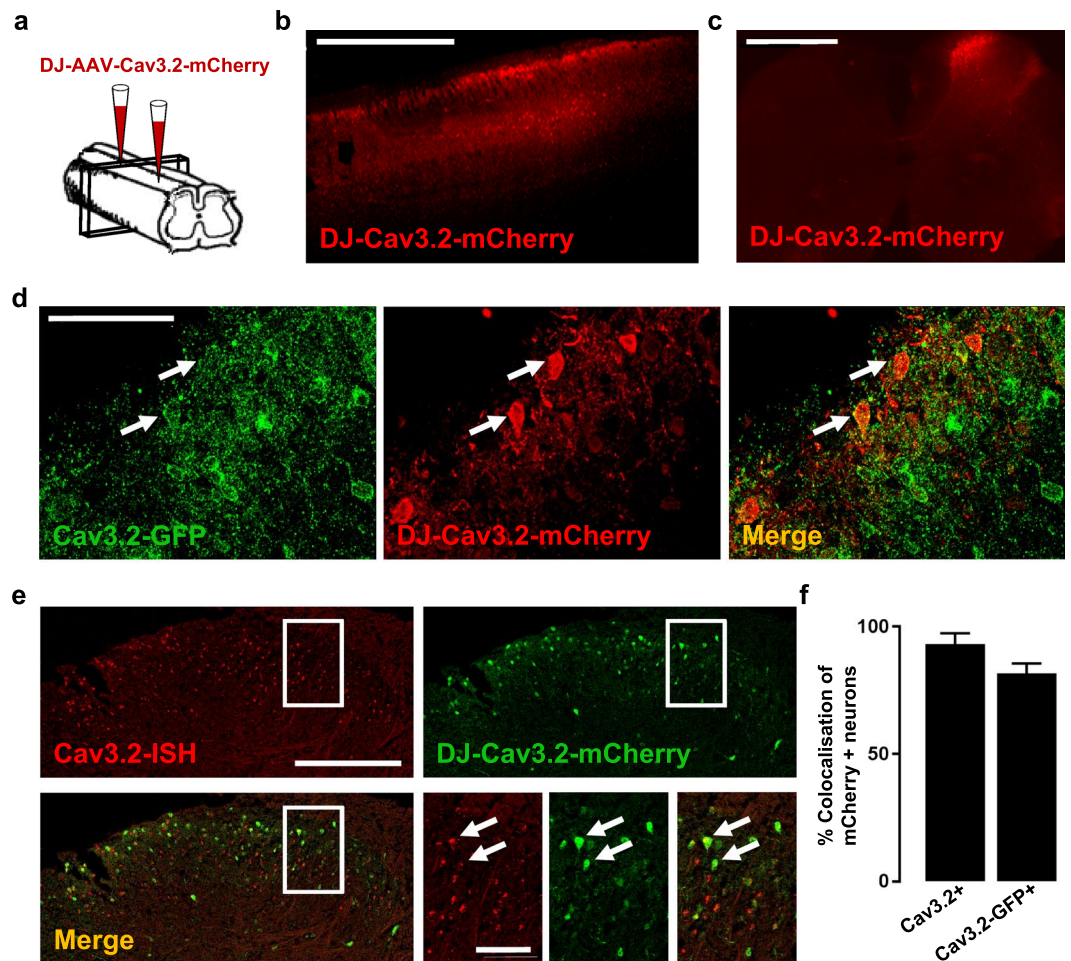


**Figure 5.** Identification of Cav3.2-expressing neurons in the lumbar spinal cord in adult mice. (A) Schema of the injection protocol, adapted from Inquimbert *et al.*<sup>39</sup>. (B,C) Detection of mCherry expression in a parasagittal (B) and a frontal (C) spinal cord slice three weeks after intraspinal injections of AAV-DJ-Cav3.2-mCherry virus in wildtype mice. (D) Detection of GFP (green) and mCherry (red) expressions by immunofluorescence in a frontal spinal cord section three weeks after intraspinal injections of AAV-DJ-Cav3.2-mCherry virus in a Cav3.2<sup>GFP-Flox</sup> KI mouse. Co-expression is indicated (arrows). (E) Detection of Cav3.2 mRNA expression (red) by *in situ* hybridization and of mCherry expression (green) by immunofluorescence in a frontal spinal cord section three weeks after intraspinal injection of AAV-DJ-Cav3.2-mCherry virus in a wildtype mouse. Co-expression is indicated (arrows). (F) Mean colocalizations between mCherry-positive neurons and either Cav3.2 mRNA in wildtype mice or GFP in Cav3.2<sup>GFP-Flox</sup> KI mice. Bars are the means and lines are the SEM from 2 and 4 mice in immunofluorescence and *in situ* hybridization experiments, respectively. Scale bars: B (1 mm), C (500  $\mu$ m), D (50  $\mu$ m), E (200  $\mu$ m, 50  $\mu$ m).

(Fig. 6A). The current-voltage relationship of this voltage-sensitive calcium current plotted at low membrane voltages was consistent with a low threshold calcium channel<sup>28</sup> in mCherry-positive neurons ( $n = 7$ , Fig. 6A) like in unidentified LII neurons encompassing Cav3.2-positive and negative neurons (Supplementary Fig. S4). In the current-clamp configuration, the peak amplitudes of the subthreshold rebounds were similar in Cav3.2-expressing neurons ( $7.6 \pm 0.7$  mV,  $n = 32$ , Fig. 6B) as compared to unidentified neurons ( $7.8 \pm 0.6$  mV,  $n = 57$ , Fig. 6B). Their time-to-peak was lengthened (unidentified neurons,  $139 \pm 8$  ms,  $n = 57$ , and Cav3.2-expressing neurons,  $193 \pm 22$  ms,  $n = 32$ ; Mann-Whitney test,  $p < 0.001$ , Fig. 6C). Yet, T-type channels were strongly involved in these subthreshold properties, as rebounds were inhibited by puff applications of  $1 \mu$ M TTA-A2 ( $n = 6$ , Wilcoxon paired test,  $p = 0.03$ , Fig. 6D). The other two types of subthreshold activities (hyperpolarizing and passive) were present in Cav3.2-expressing neurons (Fig. 6E), although their relative proportions were different as compared to unidentified neurons (Chi<sup>2</sup> test,  $p = 0.006$ ). The electrical activity was unique in Cav3.2-expressing, rebound-exhibiting neurons. Notably, the latency of an action potential (Fig. 6F), elicited upon step-depolarization, was shorter in rebound-exhibiting neurons ( $58.6 \pm 7.4$  ms,  $n = 31$ ) as compared to hyperpolarizing- ( $168 \pm 20$  ms,  $n = 29$ ) and passive-type of neurons ( $244 \pm 47$  ms,  $n = 31$ ). Accordingly, the action potential threshold (Fig. 6G) was significantly lower in rebound-exhibiting neurons ( $-38.3 \pm 1.1$  mV) as compared to hyperpolarizing- ( $-32.6 \pm 0.7$  mV) and passive-type of neurons ( $-32.2 \pm 0.7$  mV). The time-to-peak of this action potential was also different in rebound-exhibiting neurons ( $2.57 \pm 0.3$  ms) as compared to the others (respectively  $1.82 \pm 0.2$  and  $1.80 \pm 0.2$  ms,

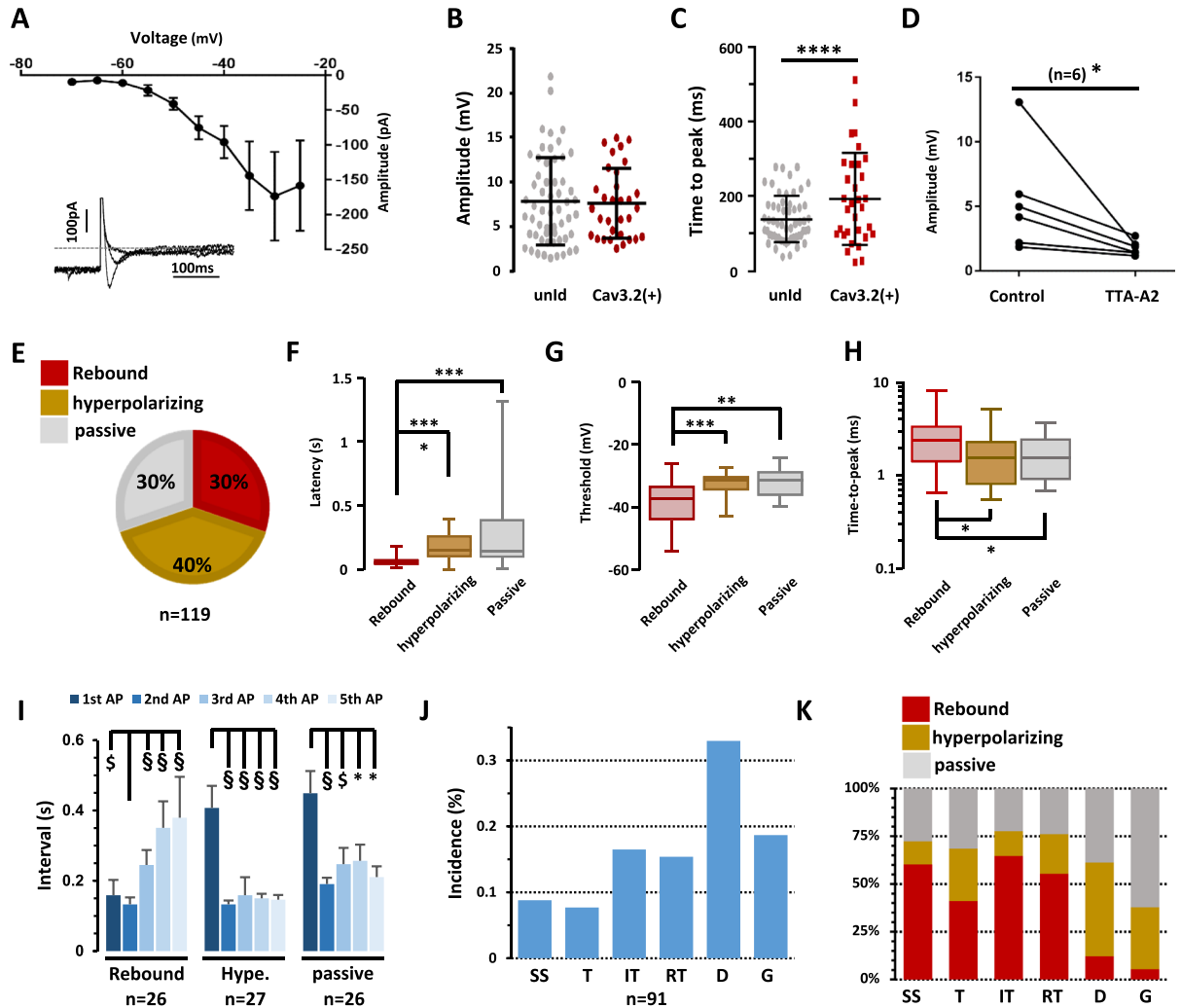


**Figure 6.** Electrophysiological properties of Cav3.2-expressing neurons in the LII of the spinal cord of adult mice. **(A)** Mean current-voltage relationship of a low-voltage activated calcium current in Cav3.2-expressing neurons. Symbols are the means and lines are the SEM from 7 LII neurons. **Inset**, typical inward currents evoked from  $-90$  mV to  $-60$ ,  $-50$  and  $-40$  mV. The extracellular medium contained  $100 \mu\text{M}$   $\text{CdCl}_2$ . **(B)** Amplitude and **(C)** time to peak of the rebound shaped depolarisations in Cav3.2-mCherry neurons ( $n = 32$ ) as compared to unidentified neurons ( $n = 57$ ). Lines are means and SEM, and dots are the individual values.  $***p < 0.001$  using a Mann-Whitney test. **(D)**  $1 \mu\text{M}$  TTA-A2 inhibited the rebound-shaped subthreshold depolarisation of LII Cav3.2-expressing neurons.  $*p = 0.01$  using a Wilcoxon paired test. **(E)** Proportions of the subthreshold properties of Cav3.2-expressing neurons. **(F–H)** Box and whiskers representations of action potential latency **(F)**, threshold **(G)**, and time-to-peak **(H)** in Cav3.2-mCherry neurons exhibiting rebounds ( $n = 32$ ), hyperpolarizing- ( $n = 28$ ) and passive-depolarisation profiles ( $n = 33$ ), as indicated.  $***p < 0.005$ ;  $**p < 0.01$ ;  $*p < 0.05$ , using a Mann-Whitney test. Action potential properties were analysed as in Fig. S3, and kinetics of depolarisations were triggered as in Fig. 4A. **(I)** Mean intervals showed a selective pairing of the first two action potentials in Cav3.2-expressing neurons with rebound subthreshold activity. Bars are the means and lines are the SEM. Significances are indicated as:  $\$p < 0.001$ ;  $\$p < 0.005$ ;  $*p < 0.05$ , using a Wilcoxon paired test. **(J)** Firing patterns of LII mCherry-positive neurons from AAV-DJ-Cav3.2-mCherry injected mice recorded in the current clamp mode of the whole-cell patch clamp technique (as in Fig. S3). **(K)** Relationships between firing patterns and subthreshold behaviors. SS (Single spiking), T (Transient), IT (Irregular Tonic), RT (Regular Tonic), D (Delayed) and G (Gap), see Fig. S3 for explanations. Dots are the means and lines are the SEM.

in hyperpolarizing- and passive-type of neurons, Fig. 6H). When examining the following action potentials, rebound-exhibiting neurons showed a pairing of the first two action potentials, like in the unidentified population ( $n = 26$ , Wilcoxon paired tests, Fig. 6I). This property was not present in the two other populations of Cav3.2-expressing neurons, where the delay of the first action potential was distinguishable from the other intervals (respectively  $n = 27$  and  $26$ , Wilcoxon paired tests, Fig. 6I). Cav3.2-expressing neurons displayed the various firing patterns, as seen in unidentified LII neurons (Fig. 6J, and Supplementary Tables 5 and 6) and there was no all-or-none association between a subthreshold activity and a firing pattern, although rebound-exhibiting neurons tended to harbor transient firing behaviors, while action potentials were more likely delayed in



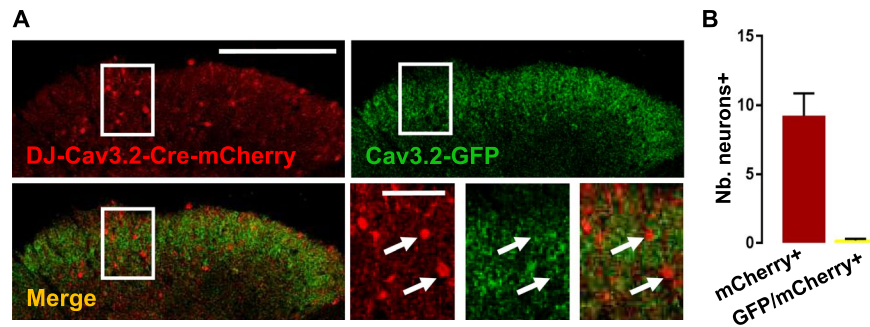


**Figure 7.** Selective deletion of Cav3.2 in the spinal cord of Cav3.2-GFP mice. (A) DH of the spinal cord slice from an adult Cav3.2-GFP mouse injected with a AAV-DJ-Cav3.2-Cre-mCherry and processed for immunodetections of GFP (green) and mCherry (red). mCherry-positive neurons lacked GFP expression as pointed out by the arrows in the expanded views of the box showed on the widest images. (B) Numbers of neurons expressing either mCherry alone or both GFP and mCherry per slice. Bars are the means and lines are the SEM of counts in 2 adult mice. Scale bars: A (200  $\mu$ m), (50  $\mu$ m).

hyperpolarizing-neurons (Fig. 6K). Collectively, these data suggest that Cav3.2-expressing neurons were not enriched with T-type calcium currents and T-type dependent firing patterns, as compared to unidentified LII neurons. This might be explained by a significant expression of Cav3.1 and Cav3.3 channels in Cav3.2-negative DH neurons<sup>27</sup>. Nevertheless, Cav3.2 seemed tightly involved in the subthreshold and suprathreshold properties of Cav3.2-expressing neurons.

**Deletion of Cav3.2 in the LII neurons of the spinal cord.** Not surprisingly, Cav3.1 and Cav3.3 mRNAs could be detected in Cav3.2-expressing neurons (Supplementary Fig. S7). Like in primary afferent neurons<sup>14,17,18</sup>, ablation of Cav3.2 expression was therefore necessary for understanding its specific roles in the adult lumbar spinal cord. A virus encoding Cre-recombinase-IRES-mCherry under the control of Cav3.2 promoter was injected into the spinal cords of Cav3.2<sup>GFP-Flox</sup> KI mice. As shown in Fig. 7A, the expression of Cav3.2-GFP was eliminated in Cre-recombinase- and mCherry-expressing neurons, and none of the mCherry-positive neurons were GFP-positive (Fig. 7B). Some cell bodies were GFP-positive and did not express mCherry (Fig. 7C) as expected in neurons that did not take up, nor express the AAV.

The properties of mCherry-expressing neurons, that had lost the expression of Cav3.2-GFP, were then examined. Cav3.2 ablation did not change either the rheobase of the neurons ( $52 \pm 2$  pA,  $n = 91$ , and  $70 \pm 10$  pA,  $n = 33$ , with and without Cav3.2, respectively). The kinetics of the action potentials were modified by the deletion of Cav3.2 (Fig. 8A–E). In the typical examples of Fig. 8A, the action potential of a Cav3.2-deleted neuron was more ample and faster than in a Cav3.2-expressing neuron. On average, half-width and time-to-peak were smaller (Fig. 8B,C) in Cav3.2-deleted neurons. In addition, both the threshold potential (Fig. 8D) and the peak potential (Fig. 8D) were shifted in Cav3.2-deleted neurons, whereas the after-hyperpolarization potential was not significantly increased (Fig. 8D). Cav3.2 was not only important for suprathreshold but also subthreshold properties since: (1) the proportions of rebound-exhibiting neurons and of hyperpolarizing neurons were decreased in Cav3.2-ablated neurons (Fig. 8E), as compared to Cav3.2-expressing neurons (see Fig. 6E) at the expense of passive-type of behavior (Chi<sup>2</sup> test,  $p < 0.0001$ ), and (2) as shown in the example of Fig. 8F, the remaining rebounds were barely detectable in Cav3.2-ablated neurons ( $3.0 \pm 0.4$  mV,  $n = 6$ , Fig. 8G) as compared to Cav3.2-expressing neurons (Fig. 8G, same data as in Fig. 6B), without alterations of their kinetics (Fig. 8H).

Cav3.2 ablation also impaired the overall firing of LII neurons. The profile of the firing of the first five action potentials was selectively modified in rebound-exhibiting neurons, as it did not show the pairing effect at the onset of activity (Fig. 8I), with the interval of the second action potential being variable from cell to cell. Yet, the latency of the first action potential was still shorter in rebound exhibiting neurons as compared to the two other populations (Fig. 8I). The firing patterns were also modified in Cav3.2-ablated neurons. The number of neurons exhibiting higher activities at the beginning of the pulse was diminished, as single spiking, transient and irregular tonic patterns were greatly down-sized in the distribution ( $n = 34$ , Fig. 8J). Thus, regular tonic and delayed patterns dominated this distribution. Finally, some relationships between subthreshold and suprathreshold properties were more apparent: most rebound-exhibiting neurons fired with a regular tonic pattern, and all hyperpolarizing neurons had delayed electrical activity, while passive neurons distributed in many classes (Fig. 8K). Note that the gap firing mode was equally represented in the three classes of neurons. Altogether, these results suggest a critical role of Cav3.2 channels in the subthreshold and suprathreshold properties of Cav3.2-expressing neurons of the LII of the spinal cord.

**Deletion of Cav3.1 in the LII neurons of the spinal cord.** The phenotype of Cav3.2-ablated LII neurons might not be selective since some of them can also express Cav3.1 and Cav3.3 (see Supplementary Fig. S7), and T-type channels might reciprocally potentiate each other's activity. This question was examined in Cav3.2-expressing LII neurons of Cav3.1 knockout mice<sup>51</sup>.

The absence of Cav3.1 in Cav3.2-expressing neurons did not change the properties of the action potentials in LII of the spinal cord (Fig. 9A–C), in marked contrast with the deletion of Cav3.2 described above. In addition, action potential firing was strongly dependent upon the activity of T-type channels, as shown in the experiment

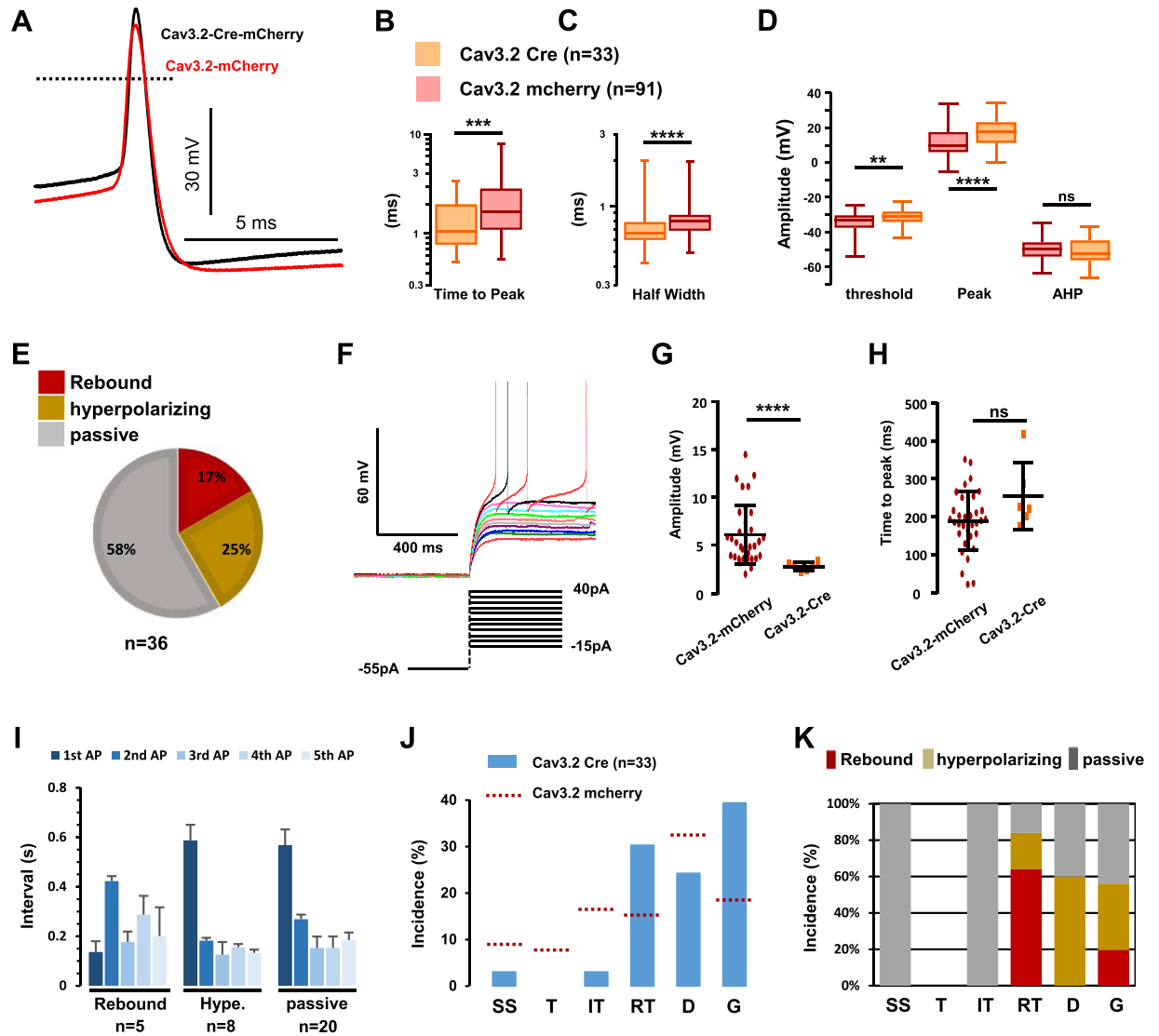


**Figure 8.** Electrophysiological properties of LII neurons lacking Cav3.2. (A) Raw traces of action potentials recorded in a Cav3.2-expressing neuron (red line) and a Cav3.2-deleted neuron (black line). (B–D) Box and whiskers representations of action potentials' time-to-peak (B), half width (C), and amplitudes (D) in mCherry-expressing neurons from either AAV-DJ-Cav3.2-mCherry injected mice (red) or AAV-DJ-Cav3.2-Cre-mCherry injected Cav3.2<sup>GFP-Flox</sup> KI mice (orange). Significance \*\*\*\* $p < 0.001$ ; \*\*\* $p < 0.005$ ; \*\* $p < 0.01$ , using a Mann Whitney test. (E) Proportions of the subthreshold properties of Cav3.2-deleted neurons. (F) Voltage traces of subthreshold and supra-threshold properties of a Cav3.2-deleted LII neuron with rebound-type depolarisation. (G,H) Amplitudes (G) and time-to-peak (H) of the subthreshold rebounds in Cav3.2-positive neurons (red dots,  $n = 34$ ) and Cav3.2-deleted neurons (orange dots,  $n = 5$ ). Lines are mean and SEM. (I) Mean intervals showed no organization of the firing in Cav3.2-deleted neurons. Bars are the means and lines are the SEM. Significances are indicated as: \*\*\*\* $p < 0.0001$ ; \*\*\* $p < 0.001$ ; \*\* $p < 0.01$ ; \* $p < 0.05$ , using a Wilcoxon paired test. (J) Firing patterns in Cav3.2-deleted LII neurons from AAV-DJ-Cav3.2-Cre-mCherry injected Cav3.2<sup>GFP-Flox</sup> KI mice, recorded in the current clamp mode of the whole-cell patch clamp technique. The dotted lines show these proportions in Cav3.2-expressing neurons (from Fig. 6J). (K) Relationships between firing patterns and subthreshold behaviors in Cav3.2-deleted LII neurons ( $n = 36$ ). (J,K) SS (Single spiking), T (Transient), IT (Irregular Tonic), RT (Regular Tonic), D (Delayed) and G (Gap), see Fig. S3 for explanations.

of Fig. 9D where superfusion with TTA-A2 ( $2 \mu\text{M}$ ) abolished firing induced by a current injection from  $-90 \text{ mV}$ . On average, TTA-A2 superfusion quickly blunted the excitability of Cav3.2-expressing neurons lacking Cav3.1 ( $n = 8$ , Fig. 9E) and significantly increased the first action potential latency in trials where firing was observed (from  $195 \pm 35$  to  $224 \pm 34 \text{ ms}$ ,  $n = 7$ ,  $p = 0.02$ , Wilcoxon paired test, (Fig. 9F). Furthermore, the distribution of the subthreshold activities was almost superimposable in Cav3.2-expressing neurons (see Fig. 6E) and in Cav3.2-expressing neurons lacking Cav3.1 (Fig. 9G). Accordingly, the maximal amplitudes (Fig. 9H) and the times-to-peak (Fig. 9I) of the rebounds induced by step-depolarization were similarly distributed in the 3 to 15 mV range in Cav3.2-expressing with or without Cav3.1. The distribution of the firing patterns was not greatly

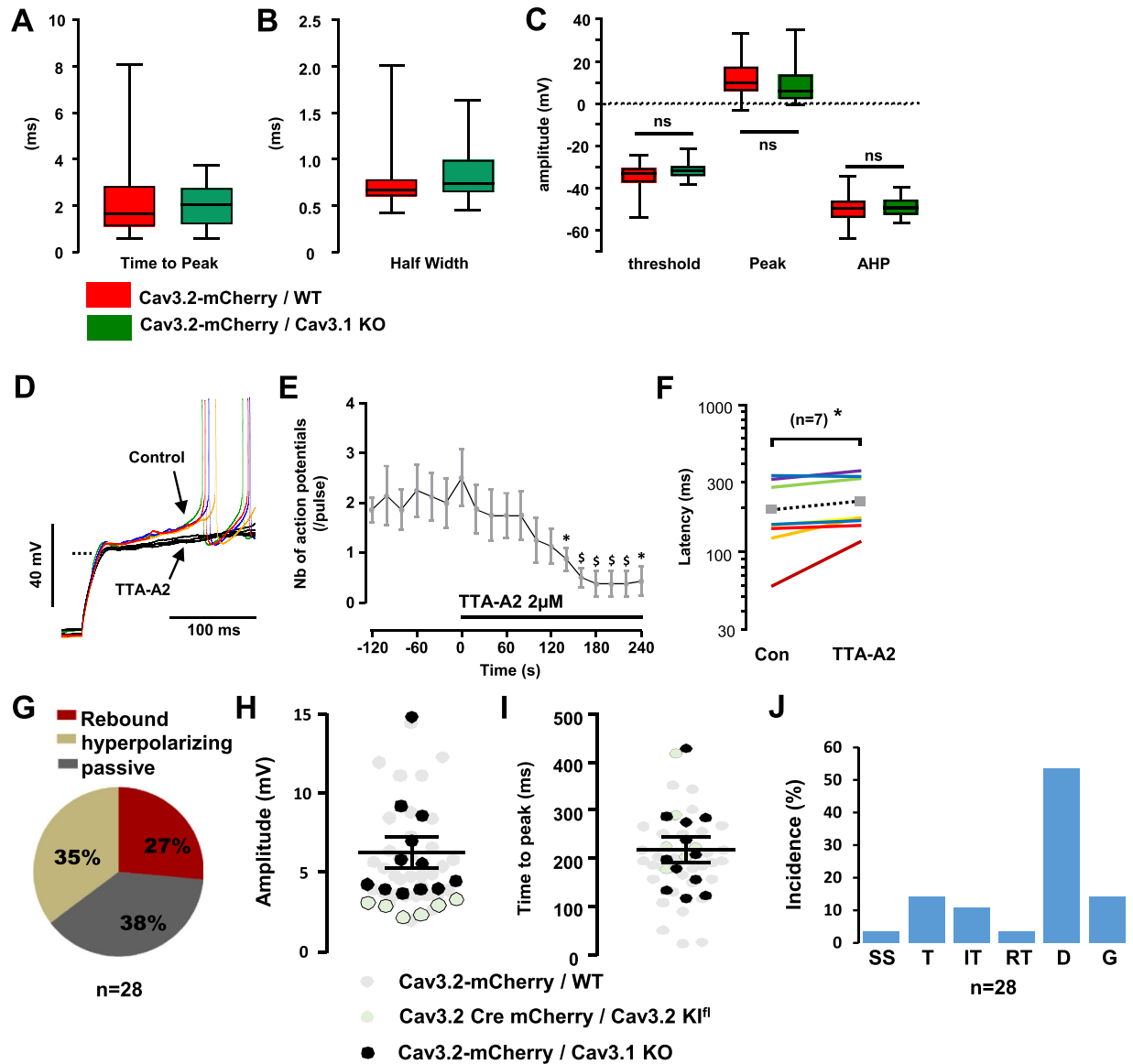


**Figure 9.** Electrophysiological properties of Cav3.2-expressing LII neurons lacking Cav3.1. (**A–C**) Box and whiskers representations of action potential's time-to-peak (**A**), half width (**B**), and amplitudes (**C**) in mCherry-expressing neurons from either AAV-DJ-Cav3.2-mCherry injected wild-type mice (red, from Fig. 6) or AAV-DJ-Cav3.2-mCherry injected Cav3.1 knockout mice (green). In (**B** and **C**): \* $p < 0.01$ ;  $^{\dagger}p < 0.05$ , using a Wilcoxon paired test. (**D**) Raw voltage traces in a mCherry positive neuron, in the absence (colored lines) and presence of 2 μM TTA-A2 (black lines), recorded in a Cav3.1 knockout mouse injected with the AAV-DJ-Cav3.2-mCherry. Steps were elicited from  $\sim -100$  mV; the dotted line indicates  $-60$  mV. (**E**) Mean number of action potentials triggered during a 200ms-long pulse (as shown in (**D**)), in the absence and presence of 2 μM TTA-A2 (as indicated by the solid line), in 7 Cav3.2-positive/Cav3.1-negative neurons. Symbols are the means and lines are the SEM. (**F**) Mean latency of the first action potential (same experiments as in **E**) triggered in the absence and presence of 2 μM TTA-A2 (as shown by the lines), in 7 Cav3.2-positive/Cav3.1-negative neurons. Symbols are the means. (**G**) Proportions of the subthreshold properties of Cav3.2-positive/Cav3.1-negative neurons. (**H,I**) Amplitudes (**H**) and time-to-peak (**I**) of the suprathreshold rebounds in Cav3.2-positive/Cav3.1-negative LII neurons (black dots,  $n = 12$ ). Similar results from Cav3.2-expressing neurons (grey dots, from Fig. 6) and from Cav3.2-deleted neurons (white dots, from Fig. 6) are shown for a comparison. Lines are mean and SEM. (**J**) Firing patterns in Cav3.2-positive/Cav3.1-negative LII neurons, recorded in the current clamp mode of the whole-cell patch clamp technique. SS (Single spiking), T (Transient), IT (Irregular Tonic), RT (Regular Tonic), D (Delayed) and G (Gap), see Fig. S3 for explanations.

altered in Cav3.1 knockout mice since 1) immediate firing (single spiking, transient and irregular tonic, Fig. 9J) amounted to  $\sim 29\%$ , and was close to the 32% seen in Cav3.2-expressing neurons (see Fig. 6J) and 2) delayed and gap firing patterns were as represented in Cav3.2-expressing LII neurons with or without Cav3.1 (respectively, 50% and 68%). Yet, the downsizing of the regular tonic firing pattern from 15% to 4% of the Cav3.2-expressing



neurons (compare Figs 6J with 9J) was opposite to the effect of Cav3.2 ablation (30%, in Fig. 8J). Altogether, these data show that spinal deletion of Cav3.2 has profound effects on the excitability of most classes of LII neurons while Cav3.1 deletion does not recapitulate these changes.

## Discussion

The Cav3.2<sup>GFP-Flox</sup> KI mouse was instrumental in deciphering the role of Cav3.2 in primary afferent neurons during chronic pain<sup>14</sup>. Here, this mouse model was used as a genetic tool for identifying Cav3.2 expressing neurons and for ablating them in LII of the spinal cord where Cav3.2 was found to play an important, and specific role in the subthreshold and suprathreshold properties.

**Synaptic transmissions.** Primary afferent fibers, including the C-LTMR and the A $\delta$ -LTMR, express Cav3.2 and project to the DH of the spinal cord<sup>14,15,52,53</sup>. GFP detection in the DH of the Cav3.2<sup>GFP-Flox</sup> KI mouse suggests that Cav3.2 has a presynaptic role<sup>14</sup>. Indeed, projection neurons of the superficial lamina I are modulated by primary afferent fibers in a T-type dependent manner<sup>6,8</sup>, that is impaired in Cav3.2 knockout mice<sup>10</sup>. In contrast, mEPSCs were not significantly modified by T-type channel inhibitors in LII neurons. There is a gap between these sets of data: the small population of projection neurons, which is rather homogenous<sup>54</sup>, was examined after retrograde labeling<sup>6,8,10</sup>, while the current data were obtained in unidentified LII neurons, that is, a heterogeneous population where some, rather than all, excitatory inputs might be Cav3.2-dependent<sup>5,9,11</sup>. The role of Cav3.2 in glutamatergic transmission will have to be examined in targeted, well-defined, LII neurons, possibly in combination with cell-type specific activation of primary afferent neurons. Surprisingly, TTA-A2 slowed mIPSCs in LII neurons, and the selective inhibition of mIPSC frequency was suggestive of a presynaptic site of action of the T-type channel inhibitor. Note that the use of TTA-A2 at concentrations in the micromolar range precludes this compound from blocking high-voltage activated calcium channels in multicellular preparations<sup>55,56</sup>. Altogether, the distribution of Cav3.2 at inhibitory synapses of LII neurons appeared more homogenous than at excitatory synapses. It will be interesting to investigate if these synapses arise from local interneurons and/or from descending inhibitory pathways. Note that T-type channel inhibition does not seem as tightly involved in the GABAergic neurotransmission in other preparations<sup>9,10</sup>. Some methodological differences between these and our study might be tested in the future (namely, animal species and age, recording conditions including pharmacology).

**Action potential properties.** As suggested by the dense Cav3.2 labelling of neuronal cell bodies in LII, the intrinsic properties of LII neurons involved a contribution from Cav3.2. First, the early steps of the action potential (time-to-peak, threshold and peak amplitudes) were modified by the ablation of Cav3.2, as expected for a protein involved in subthreshold properties. Cav3.2 ablation not only diminished the proportion of rebound-exhibiting neurons and the amplitude (if any) of this rebound, since some suprathreshold properties of the hyperpolarizing and the passive neurons were also altered in Cav3.2 deleted LII neurons (Supplementary Table 7). Accordingly, the proportion of LII neurons with T-type calcium currents (~75%) is larger than the rebound-exhibiting population (~30%). In apparent contrast, Cav3.2 ablation modified neuronal excitability without changing action potential threshold in A $\delta$ -LTMR cell bodies<sup>57</sup>. Keeping in mind that Cav3.2 can be found at the axon initial segment, others have suggested that its contribution to neuronal spiking might have profound, albeit non-conventional, effects<sup>58,59</sup>. For a comparison, the deletion of Cav3.1 did not mimic these changes, suggesting that Cav3.1 might be relevant in other compartments of the LII neurons. Alternately, Cav3.1 might not have a homogenous role in Cav3.2-expressing LII neurons. Second, Cav3.2 ablation shortened the half-width of the action potential in LII neurons, and this occurred with a significant change of the AHP in rebound-exhibiting neurons only (Supplementary Table 7). T-type channel inhibition decreases the amplitude of the AHP in other neurons as well<sup>6,60</sup>. Third, the mean action potential latency was not significantly increased in Cav3.2-ablated LII neurons as compared to Cav3.2-expressing neurons despite the subthreshold role of Cav3.2. The mean action potential latency was also similar in A $\delta$ -LTMR cell bodies of either Cav3.2-deleted mice or wild-type mice<sup>57</sup>. Altogether these data establish that Cav3.2 has unique roles in the LII neurons, which should be examined further in the multiple subpopulations found by Zeisel *et al.*<sup>61</sup>.

**Firing patterns and spike coding.** The firing patterns of neurons are heterogeneous in LII<sup>12,29,30,32,34</sup>, and are not less heterogeneous in Cav3.2-expressing neurons. Because of their inactivation properties, T-type calcium channels are first viewed as supporting transient activities<sup>50,62</sup>. Cav3.2 ablation indeed lowered the population of LII neurons with immediate activity, encompassing single-spiking, transient, and irregular tonic patterns. Cav3.2-ablated neurons exhibited mostly delayed and gap patterns. Being driven by transient potassium channels, their firing delays were expected to be exacerbated, if anything, in Cav3.2-ablated neurons<sup>32,63</sup>. The transition from transient behaviors to more regular tonic patterns might be related to the simultaneous decrease in the proportion of rebound-exhibiting neurons and in the decrease in the amplitude of the rebound in the remaining neurons. T-type calcium channels also contribute to tonic firing when they generate a tonic “window” depolarisation<sup>12,13,64,65</sup>. In thalamic neurons, where peak T-type currents are in the nA range, the tonic contribution of T-type channels is ~2mV<sup>36</sup>. Since T-type currents were much smaller (10–100 pA range) in LII neurons, it was not surprising that the proportions of regular firing patterns (regular tonic + delayed) and of irregular patterns (irregular tonic + gap) were similar in Cav3.2-expressing neurons and Cav3.2-ablated neurons. A putative tonic contribution of Cav3.2 to the resting potential might better be examined in combination with varying synaptic strengths<sup>64</sup>.

Cav3.2 likely plays a role in the coincidence detector function of LII, as suggested by the result of Cav3.2-ablation. First, spike initiation being influenced by T-type channels, variations or regulations of Cav3.2 activity will control the precision of the temporal summation of synaptic inputs<sup>64</sup>. Second, delayed excitation (a rebound of the membrane potential triggered by inhibitory transmission) is strongly dependent upon T-type

channels activity<sup>31,66</sup>, and might largely depend upon Cav3.2 in LII neurons (this study). Third, the downstream transmission of the sensory signal depends on neuronal firing patterns. Single spiking patterns, blunted in Cav3.2-ablated neurons, convey spike time precision and the opportunity in pairing synaptic inputs on postsynaptic neurons<sup>64,67</sup>. Altogether, Cav3.2 ablation perturbed millisecond coding properties of LII neurons, required for temporal neural codes<sup>68</sup>.

The action potential pairing, eliminated by Cav3.2 ablation in LII neurons, shared some, but not all, properties with other neurons. Indeed, delayed doublet spiking also occurs in sensory neurons of an electric fish, but this is a TTX-sensitive event which terminates bursts<sup>69</sup>. Doublet spiking is followed by an AHP which silences electrical activity in motoneurons, and this might facilitate force generation<sup>70</sup>. In mature granule neurons of the dentate gyrus, Cav3.2 supports action potential pairing within tenth of ms, while T-type channel antagonists or Cav3.2 genetic ablation lengthen this interval to no more than 75 ms<sup>71</sup>. In the cerebellum, long term depression at the parallel fiber – Purkinje neuron excitatory synapse is better induced by a fast pairing of parallel fiber stimulation (interval 60 ms)<sup>72</sup>. These doublets, whose functions are identified, are much faster than those elicited by T-type dependent rebounds in LII neurons and fall into the 50–200 ms range. Yet, these kinetics fit with the hypothesis of Cav3.2 participating in paired pulse facilitation/depression at inhibitory synapses in the DH of the spinal cord<sup>67</sup>. In support for this hypothesis, TTA-A2 blunted the spontaneous inhibitory currents in LII neurons in a manner consistent with a presynaptic mode of action. However, the other T-type channels likely participate in synaptic inhibition as well, because Cav3.2 was not common in Pax2-expressing neurons. Recording from identified synapses, which is becoming feasible with the classification of neuronal subpopulations<sup>61</sup>, will be required in resolving these issues.

**Functional specificity.** Some Cav3.2-expressing neurons expressed Cav3.1 or Cav3.3 in the spinal cord. Despite similar biochemical and electrophysiological characteristics, T-type channels can be discriminated from each other<sup>73,74</sup>. In addition, their subcellular localizations are not always overlapping<sup>75</sup>. In LII neurons, Cav3.1 and Cav3.2 were not redundant since the subthreshold and suprathreshold properties of Cav3.2-expressing neurons were similar in Cav3.1 knockout mice and in wildtype mice. A putative cooperativity between Cav3.1 and Cav3.2 did not take place in LII neurons either, as Cav3.1 deletion had minimal effects (if any) on excitability while Cav3.2 deletion seemed to eliminate most if not all signatures of T-type calcium channels. Future sets of experiments, including afferent synaptic activation for instance, might challenge this conclusion. In addition, the  $\sim 3.0 \pm 0.4$  mV mean rebound remaining in Cav3.2-ablated neurons (see Fig. 8G) might not be negligible, and its putative mechanism remains to be clarified (the residual rebound in the presence of TTA-A2 being in the  $\sim 1$  mV range). The unique role of Cav3.2 was also suggested by the unusual proportion of passive subthreshold behaviors in Cav3.2-deleted LII neurons. Another comparison, between the distributions of subthreshold properties in unidentified neurons and Cav3.2-expressing neurons suggest an electrogenic role of either Cav3.1 and/or Cav3.3 in Cav3.2-negative neurons notably because rebounds were more common in unidentified neurons. The kinetics of the rebounds, shorter in unidentified neurons, again suggested distinct properties between Cav3.2-positive and Cav3.2-negative LII neurons. Future experiments will be needed in deciphering the roles of Cav3.1 and Cav3.3 in the spinal cord, keeping in mind that inactivation of their genes does not induce analgesia, so far<sup>16,17</sup>.

Our immunostaining and the *in situ* hybridization experiments clarified the heterogeneity of the Cav3.2-expressing neuronal population. So far, Cav3.2 colocalized mainly with excitatory neurons in the general population as well as in each of the subpopulations examined, but the PV neurons. Importantly, Cav3.2 is present in almost each PKC $\gamma$  interneuron, and these neurons are on the pathway of non-nociceptive information to the projection neurons of lamina I<sup>21–26</sup>. Interestingly, a large population of CR neurons (41%) is also Cav3.2-positive, and this proportion is somewhat higher than suggested by the patch-clamp recordings of Smith *et al.*<sup>32</sup>. Unlike PKC $\gamma$  interneurons, CR neurons seem to be involved in inflammatory pain and unrelated to the onset and development of mechanical allodynia<sup>76</sup>. The role(s) of Cav3.2 in CR is/are as yet unknown, and the development of new transgenic mice models and/or new AAV will be useful in examining these functions. In contrast to these Cav3.2-positive neurons that allow the propagation of the allodynic signal to the projection neuron, the PV neurons which gates this pathway<sup>26</sup> did not express Cav3.2. Although the understanding of T-type channel functions within the spinal cord still remains to be fully elucidated, they are likely to tune the excitability of some spinal neuronal networks, the pharmacological modulation of which might be of therapeutic importance.

## References

- Choi, S. *et al.* Attenuated pain responses in mice lacking Ca(V)3.2 T-type channels. *Genes Brain Behav* **6**, 425–431 (2007).
- Shen, F. Y. *et al.* Alleviation of neuropathic pain by regulating T-type calcium channels in rat anterior cingulate cortex. *Mol Pain* **11**, 7 (2015).
- Kerckhove, N. *et al.* Ca(v)3.2 calcium channels: the key protagonist in the supraspinal effect of paracetamol. *Pain* **155**, 764–772 (2014).
- Snutch, T. P. & Zamponi, G. W. Recent advances in the development of T-type calcium channel blockers for pain intervention. *Br J Pharmacol* **175**, 2375–2383 (2017).
- Bao, J. P., Li, J. J. & Perl, E. R. Differences in Ca<sup>2+</sup> channels governing generation of miniature and evoked excitatory synaptic currents in spinal laminae I and II. *J Neurosci* **18**, 8740–8750 (1998).
- Ikeda, H., Heinke, B., Ruscheweyh, R. & Sandkuhler, J. Synaptic plasticity in spinal lamina I projection neurons that mediate hyperalgesia. *Science* **299**, 1237–1240 (2003).
- Ikeda, H. *et al.* Synaptic amplifier of inflammatory pain in the spinal dorsal horn. *Science* **312**, 1659–1662 (2006).
- Drdla, R. & Sandkuhler, J. Long-term potentiation at C-fibre synapses by low-level presynaptic activity *in vivo*. *Mol Pain* **4**, 18 (2008).
- Yuan, W. X., Chen, S. R., Chen, H. & Pan, H. L. Stimulation of alpha(1)-adrenoceptors reduces glutamatergic synaptic input from primary afferents through GABA(A) receptors and T-type Ca(2+) channels. *Neuroscience* **158**, 1616–1624 (2009).
- Jacus, M. O., Uebele, V. N., Renger, J. J. & Todorovic, S. M. Presynaptic Ca(V)3.2 Channels Regulate Excitatory Neurotransmission in Nociceptive Dorsal Horn Neurons. *J Neurosci* **32**, 9374–9382 (2012).
- Garcia-Caballero, A. *et al.* The deubiquitinating enzyme USP5 modulates neuropathic and inflammatory pain by enhancing Cav3.2 channel activity. *Neuron* **83**, 1144–1158 (2014).

12. Wu, J. *et al.* Cell-Type Specific Distribution of T-Type Calcium Currents in Lamina II Neurons of the Rat Spinal Cord. *Front Cell Neurosci.* **17**(12), 370 (2018).
13. Liao, Y. F., Tsai, M. L., Chen, C. C. & Yen, C. T. Involvement of the Cav3.2 T-type calcium channel in thalamic neuron discharge patterns. *Mol Pain* **7**, 43 (2011).
14. Francois, A. *et al.* The Low-Threshold Calcium Channel Cav3.2 Determines Low-Threshold Mechanoreceptor Function. *Cell Rep* **10**, 370–382 (2015).
15. Bernal Sierra, Y. A., Haseleu, J., Kozlenkov, A., Begay, V. & Lewin, G. R. Genetic Tracing of Cav3.2 T-Type Calcium Channel Expression in the Peripheral Nervous System. *Front Mol Neurosci* **10**, 70 (2017).
16. Marger, F. *et al.* T-type calcium channels contribute to colonic hypersensitivity in a rat model of irritable bowel syndrome. *Proc Natl Acad Sci USA* **108**, 11268–11273 (2011).
17. Bourinet, E. *et al.* Silencing of the Cav3.2 T-type calcium channel gene in sensory neurons demonstrates its major role in nociception. *EMBO J* **24**, 315–324 (2005).
18. Messinger, R. B. *et al.* *In vivo* silencing of the Ca(V)3.2 T-type calcium channels in sensory neurons alleviates hyperalgesia in rats with streptozocin-induced diabetic neuropathy. *Pain* **145**, 184–195 (2009).
19. Antal, M. *et al.* Different populations of parvalbumin- and calbindin-D28k-immunoreactive neurons contain GABA and accumulate 3H-D-aspartate in the dorsal horn of the rat spinal cord. *J Comp Neurol* **314**, 114–124 (1991).
20. Abraira, V. E. *et al.* The Cellular and Synaptic Architecture of the Mechanosensory Dorsal Horn. *Cell* **168**, 295–310 e219 (2017).
21. Torsney, C. & MacDermott, A. B. Disinhibition opens the gate to pathological pain signaling in superficial neurokinin 1 receptor-expressing neurons in rat spinal cord. *J Neurosci* **26**, 1833–1843 (2006).
22. Miraucourt, L., Dallel, S. R. & Voisin, D. L. Glycine inhibitory dysfunction turns touch into pain through PKC $\gamma$  interneurons. *PLoS One* **2**, e1116 (2007).
23. Lu, Y. *et al.* A feed-forward spinal cord glycinergic neural circuit gates mechanical allodynia. *J Clin Invest* **123**, 4050–4062 (2013).
24. Peirs, C. *et al.* Protein kinase C gamma interneurons in the rat medullary dorsal horn: distribution and synaptic inputs to these neurons, and subcellular localization of the enzyme. *J Comp Neurol* **522**, 393–413 (2014).
25. Foster, E. *et al.* Targeted ablation, silencing, and activation establish glycinergic dorsal horn neurons as key components of a spinal gate for pain and itch. *Neuron* **85**, 1289–1304 (2015).
26. Petitjean, H. *et al.* Dorsal Horn Parvalbumin Neurons Are Gate-Keepers of Touch-Evoked Pain after Nerve Injury. *Cell Rep* **13**, 1246–1257 (2015).
27. Talley, E. M. *et al.* Differential distribution of three members of a gene family encoding low voltage-activated (T-type) calcium channels. *J Neurosci* **19**, 1895–1911 (1999).
28. Ryu, P. D. & Randic, M. Low- and high-voltage-activated calcium currents in rat spinal dorsal horn neurons. *J Neurophysiol* **63**, 273–285 (1990).
29. Ruscheweyh, R. & Sandkuhler, J. Lamina-specific membrane and discharge properties of rat spinal dorsal horn neurones *in vitro*. *J Physiol* **541**, 231–244 (2002).
30. Ku, W. H. & Schneider, S. P. Multiple T-type Ca<sup>2+</sup> current subtypes in electrophysiologically characterized hamster dorsal horn neurons: possible role in spinal sensory integration. *J Neurophysiol* **106**, 2486–2498 (2011).
31. Reali, C. & Russo, R. E. Neuronal intrinsic properties shape naturally evoked sensory inputs in the dorsal horn of the spinal cord. *Front Cell Neurosci* **7**, 276 (2010).
32. Smith, K. M. *et al.* Functional heterogeneity of calretinin-expressing neurons in the mouse superficial dorsal horn: implications for spinal pain processing. *J Physiol* **593**, 4319–4339 (2015).
33. Baccam, N. *et al.* Dual-level afferent control of growth hormone-releasing hormone (GHRH) neurons in GHRH-green fluorescent protein transgenic mice. *J Neurosci* **27**, 1631–1641 (2007).
34. Grudt, T. J. & Perl, E. R. Correlations between neuronal morphology and electrophysiological features in the rodent superficial dorsal horn. *J Physiol* **540**, 189–207 (2002).
35. Clements, J. D. & Bekkers, J. M. Detection of spontaneous synaptic events with an optimally scaled template. *Biophys J* **73**, 220–229 (1997).
36. Dreyfus, F. M. *et al.* Selective T-type calcium channel block in thalamic neurons reveals channel redundancy and physiological impact of I(T)window. *J Neurosci* **30**, 99–109 (2010).
37. van Loo, K. M. *et al.* Transcriptional regulation of T-type calcium channel CaV3.2: bi-directionality by early growth response 1 (Egr1) and repressor element 1 (RE-1) protein-silencing transcription factor (REST). *J Biol Chem* **287**, 15489–15501 (2012).
38. Morgenstern, P. F., Marongiu, R., Musatov, S. A. & Kaplitt, M. G. Adeno-associated viral gene delivery in neurodegenerative disease. *Methods Mol Biol* **793**, 443–455 (2011).
39. Inquimbert, P., Moll, M., Kohno, T. & Scholz, J. Stereotaxic injection of a viral vector for conditional gene manipulation in the mouse spinal cord. *J Vis Exp* **73**, e50313 (2013).
40. Kohro, Y. E. *et al.* A new minimally-invasive method for microinjection into the mouse spinal dorsal horn. *Sci Rep* **21**, 14306 (2015).
41. Schindelin, J. *et al.* Fiji: an open-source platform for biological-image analysis. *Nat Methods* **9**, 676–682 (2012).
42. Moqrigh, A. *et al.* Expressing TrkC from the TrkA locus causes a subset of dorsal root ganglia neurons to switch fate. *Nat Neurosci* **7**, 812–818 (2004).
43. Cheng, L. *et al.* Tlx3 and Tlx1 are post-mitotic selector genes determining glutamatergic over GABAergic cell fates. *Nat Neurosci* **7**, 510–517 (2004).
44. Muller, T. *et al.* The bHLH factor Olig3 coordinates the specification of dorsal neurons in the spinal cord. *Genes Dev* **19**, 733–743 (2005).
45. Polgar, E., Shehab, S. A., Watt, C. & Todd, A. J. GABAergic neurons that contain neuropeptide Y selectively target cells with the neurokinin 1 receptor in laminae III and IV of the rat spinal cord. *J Neurosci* **19**, 2637–2646 (1999).
46. Hughes, A. S., Averill, S., King, V. R., Molander, C. & Shortland, P. J. Neurochemical characterization of neuronal populations expressing protein kinase C gamma isoform in the spinal cord and gracile nucleus of the rat. *Neuroscience* **153**, 507–517 (2008).
47. Sardella, T. C., Polgar, E., Watanabe, M. & Todd, A. J. A quantitative study of neuronal nitric oxide synthase expression in laminae I–III of the rat spinal dorsal horn. *Neuroscience* **192**, 708–720 (2011).
48. Polgar, E., Sardella, T. C., Tiong, S. Y., Locke, S., Watanabe, M. & Todd, A. J. Functional differences between neurochemically defined populations of inhibitory interneurons in the rat spinal dorsal horn. *Pain* **154**, 2606–2615 (2013).
49. Inquimbert, P. *et al.* Peripheral nerve injury produces a sustained shift in the balance between glutamate release and uptake in the dorsal horn of the spinal cord. *Pain* **153**, 2422–2431 (2012).
50. Llinas, R. R. & Steriade, M. Bursting of thalamic neurons and states of vigilance. *J Neurophysiol* **95**, 3297–3308 (2006).
51. Kim, D. *et al.* Lack of the burst firing of thalamocortical relay neurons and resistance to absence seizures in mice lacking alpha(1G) T-type Ca(2+) channels. *Neuron* **31**, 35–45 (2001).
52. Shin, J. B., Martinez-Salgado, C., Heppenstall, P. A. & Lewin, G. R. A T-type calcium channel required for normal function of a mammalian mechanoreceptor. *Nat Neurosci* **6**, 724–730 (2003).
53. Usoskin, D. *et al.* Unbiased classification of sensory neuron types by large-scale single-cell RNA sequencing. *Nat Neurosci* **18**, 145–153 (2015).
54. Al-Khater, K. M., Kerr, R. & Todd, A. J. A quantitative study of spinothalamic neurons in laminae I, III, and IV in lumbar and cervical segments of the rat spinal cord. *J Comp Neurol* **511**, 1–18 (2008).



55. Chevalier, M. *et al.* T-type calcium channels are involved in hypoxic pulmonary hypertension. *Cardiovasc Res* **103**, 597–606 (2014).
56. Kraus, R. L. *et al.* *In vitro* characterization of T-type calcium channel antagonist TTA-A2 and *in vivo* effects on arousal in mice. *J Pharmacol Exp Ther* **335**, 409–17 (2010).
57. Wang, R. & Lewin, G. R. The Cav3.2 T-type calcium channel regulates temporal coding in mouse mechanoreceptors. *J Physiol* **589**, 2229–2243 (2011).
58. Bender, K. J., Ford, C. P. & Trussell, L. O. Dopaminergic modulation of axon initial segment calcium channels regulates action potential initiation. *Neuron* **68**, 500–511 (2010).
59. Vascak, M., Sun, J., Baer, M., Jacobs, K. M. & Povolishock, J. T. Mild Traumatic Brain Injury Evokes Pyramidal Neuron Axon Initial Segment Plasticity and Diffuse Presynaptic Inhibitory Terminal Loss. *Front Cell Neurosci* **11**, 157 (2017).
60. Lambert, R. C. *et al.* Low-voltage-activated Ca<sup>2+</sup> currents are generated by members of the CavT subunit family (alpha1G/H) in rat primary sensory neurons. *J Neurosci* **18**, 8605–8613 (1998).
61. Zeisel, A. *et al.* Molecular Architecture of the Mouse Nervous System. *Cell* **174**, 999–1014 (2018).
62. Isope, P., Hildebrand, M. E. & Snutch, T. P. Contributions of T-type voltage-gated calcium channels to postsynaptic calcium signaling within Purkinje neurons. *Cerebellum* **11**, 651–665 (2012).
63. Yoshimura, M. & Jessell, T. M. Membrane properties of rat substantia gelatinosa neurons *in vitro*. *J Neurophysiol* **62**, 109–118 (1989).
64. Ratte, S., Lankarany, M., Rho, Y. A., Patterson, A. & Prescott, S. A. Subthreshold membrane currents confer distinct tuning properties that enable neurons to encode the integral or derivative of their input. *Front Cell Neurosci* **8**, 452 (2014).
65. Cain, S. M. & Snutch, T. P. Contributions of T-type calcium channel isoforms to neuronal firing. *Channels (Austin)* **4**, 475–482 (2010).
66. Boehme, R., Uebele, V. N., Renger, J. J. & Pedroarena, C. Rebound excitation triggered by synaptic inhibition in cerebellar nuclear neurons is suppressed by selective T-type calcium channel block. *J Neurophysiol* **106**, 2653–2661 (2011).
67. Zhang, W. & Schneider, S. P. Short-term modulation at synapses between neurons in laminae II-V of the rodent spinal dorsal horn. *J Neurophysiol* **105**, 2920–2930 (2011).
68. Panzeri, S., Brunel, N., Logothetis, N. K. & Kayser, C. Sensory neural codes using multiplexed temporal scales. *Trends Neurosci* **33**, 111–20 (2010).
69. Lemon, N. & Turner, R. W. Conditional spike backpropagation generates burst discharge in a sensory neuron. *J Neurophysiol* **84**, 1519–1530 (2000).
70. Mrowczynski, W., Celichowski, J., Raikova, R. & Krutki, P. Physiological consequences of doublet discharges on motoneuronal firing and motor unit force. *Front Cell Neurosci* **9**, 81 (2015).
71. Dumenieu, M. *et al.* The Low-Threshold Calcium Channel Cav3.2 Mediates Burst Firing of Mature Dentate Granule Cells. *Cereb Cortex* **28**, 2594–2609 (2018).
72. Casado, M., Isope, P. & Ascher, P. Involvement of presynaptic N-methyl-D-aspartate receptors in cerebellar long-term depression. *Neuron* **33**, 123–130 (2002).
73. Warre, R. C., McNaughton, N. C. & Randall, A. D. Differential discrimination of fast and slow synaptic waveforms by two low-voltage-activated calcium channels. *Neuroscience* **110**, 375–388 (2002).
74. Molineux, M. L. *et al.* Specific T-type calcium channel isoforms are associated with distinct burst phenotypes in deep cerebellar nuclear neurons. *Proc Natl Acad Sci USA* **103**, 5555–5560 (2006).
75. McKay, B. E. *et al.* Ca(V)<sub>3</sub> T-type calcium channel isoforms differentially distribute to somatic and dendritic compartments in rat central neurons. *Eur J Neurosci* **24**(9), 2581–2594 (2006).
76. Koch, S. C., Acton, D. & Goulding, M. Spinal Circuits for Touch, Pain, and Itch. *Annu Rev Physiol* **80**, 189–217 (2018).

## Acknowledgements

We thank the staff of the Montpellier Biocampus animal facilities for assistance with transgenic mouse lines; the staff of the Montpellier Biocampus imaging core for assistance with confocal microscopy; S. Debiesse for genotyping services; and Maud Flaceliere and Pierre Giraud for help with molecular biology experiments. We thank Dr. T. Muller (Max-Delbrück-Center for Molecular Medicine, Berlin, Germany) for the generous gift of anti Tlx3 antibodies; and Dr. V. Prévot (Inserm U1172, Lille, France) for the generous gift of the anti nNOS antibody. We thank E. Vellayoudom, G. Coiffard, Dr. S. Granier, Dr. A. Alloui for participating in early pilot experiments. We thank Dr. E. Valjent, Dr. J. Chemin, Dr. F. Agosti, P. Tarot and L. Cutando (IGF), Drs M. Heine, M. Dumenieu (Leidnitz Institute of Neurobiology, Magdeburg, Germany), Drs P. Carroll, F. Scamps (INM, Montpellier), Drs N. Leresche, R. Lambert (NPS-IBPS, Paris) for helpful discussions. These studies were supported by operating grants to E. Bourinet from the Agence Nationale de la Recherche (ANR Pain-T, and ANR C-LTMR), Institut National de la Santé et de la Recherche Médicale, Centre National de la Recherche Scientifique, Université de Montpellier, Labex ICIST, and la Fondation pour la Recherche Médicale (équipe FRM 2015); and to G.W. Zamponi from the Canadian Institutes of Health Research and the Canada Research Chairs Program. M. Candelas and A. Fruquière were supported by fellowships from the LABEX ICST and the FRM respectively.

## Author Contributions

M.C., A.R., M.A.L., C.N., A.F., E.D., C.L., C.B., S.L., E.B. and P.F.M. did the experiments; M.C., M.A.L., C.B. and P.F.M. analyzed the experiments; M.A.L., A.M., V.C., J.H. and G.W.Z. provided molecular biology resources, P.I. and Y.L.F. provided information and protocols for patch-clamp experiments; M.C., A.R., G.W.Z., E.B. and P.F.M. wrote the article; Az.M., E.B. and P.F.M. directed the work.

## Additional Information

**Supplementary information** accompanies this paper at <https://doi.org/10.1038/s41598-019-39703-3>.

**Competing Interests:** The authors declare no competing interests.

**Publisher's note:** Springer Nature remains neutral with regard to jurisdictional claims in published maps and institutional affiliations.



**Open Access** This article is licensed under a Creative Commons Attribution 4.0 International License, which permits use, sharing, adaptation, distribution and reproduction in any medium or format, as long as you give appropriate credit to the original author(s) and the source, provide a link to the Creative Commons license, and indicate if changes were made. The images or other third party material in this article are included in the article's Creative Commons license, unless indicated otherwise in a credit line to the material. If material is not included in the article's Creative Commons license and your intended use is not permitted by statutory regulation or exceeds the permitted use, you will need to obtain permission directly from the copyright holder. To view a copy of this license, visit <http://creativecommons.org/licenses/by/4.0/>.

© The Author(s) 2019